Thesis for the Degree of Licentiate of Engineering

Sparse Array Synthesis of Complex Antenna Elements

Carlo Bencivenni

CHALMERS

Department of Signals and Systems
Chalmers University of Technology

Göteborg, Sweden 2015

Sparse Array Synthesis of Complex Antenna Elements
Carlo Bencivenni

Technical report number: R006/2015
ISSN 1403-266X

Department of Signals and Systems
Antenna Systems Division
Chalmers University of Technology
SE–412 96 Göteborg
Sweden
Telephone: +46 (0)31 – 772 1000
Email: carlo.bencivenni@chalmers.se

Typeset by the author using LaTeX.

Chalmers Reproservice
Göteborg, Sweden 2015

A mia nonna

Abstract

Arrays of antennas can significantly improve the performances and extend the capabilities of single-element antennas. However, antenna arrays are expensive solutions and therefore it is critical to keep the costs to a minimum. Aperiodic arrays can minimize the number of elements and thus the costs, however their design is far more challenging than uniform arrays, for which well-known, closed-form solutions are available.

Stochastic global optimization techniques can employ complex antenna models and specifications but suffer from high computational complexity. Analytical methods, on the other hand, can handle any problem size but they are limited to simplified models and specifications.

In this thesis we propose a new deterministic method for the design of large aperiodic sparse arrays of realistic and complex antennas. The method is based on the Compressive Sensing theory which has been extended to account for EM phenomena and complex specifications.

In the first part, the hybridization of the method with the full-wave analysis is discussed. Starting from the design in the absence of mutual coupling the array is iteratively refined through an EM analysis until convergence is reached. Results for a linear array of dipoles show the successful correction for the strong coupling degradation which turns out to give rise to a reduction in the number of elements as well. For a planar array of horn antennas the effects are less pronounced but still important in the cross polar levels.

In the second part the method is extended to multi-beam optimization. The array is designed for phase scanning applications when deformations due to phase shifter quantization and mutual coupling effects are considered. Results show that the method accurately synthesizes multi-spot beamforming arrays, although an increase in the number of elements is observed.

Finally, the effects of layout and excitation symmetries have been investigated as a means to reduce the array manufacturing cost. It is shown that, by enforcing a symmetry, the design can be simplified at the expense of an increase in the number of antenna elements.

Keywords: aperiodic array, maximally sparse array, compressive sensing, mutual coupling, array signal processing, phase scanning, symmetric layout.

Preface

This thesis is in partial fulfillment for the degree of Licentiate of Engineering at Chalmers University of Technology.

The work resulting in this thesis was carried out between June 2012 and April 2015 and has been performed within the Antenna Systems Division, Department of Signals and Systems, Chalmers. Associate Professor Marianna Ivashina has been both the examiner and main supervisor, and Assistant Professor Rob Maaskant has been the co-supervisor.

The work has been supported by a grant from the Swedish Research Council (VR) and the Swedish Innovation Agency (VINNOVA).

Acknowledgments

First I would like to thank my supervisor Associate Professor Marianna Ivashina for the giving me the opportunity to work on challenging and relevant research topics. Thank you for the support, encouragement and guidance in these years. I would equally like to thank my co-supervisor Assistant Professor Rob Maaskant for the attention, commitment and time dedicated to my work. We had many interesting discussions and I am very grateful for everything you taught me. I also would like to express my appreciation to Professor Per-Simon Kildal for creating a great and friendly research environment in the Antenna Division.

I would like to recognize the CHASE center and our partners, RUAG, Ericsson and KTH, for supporting the project. In particular I would like to thank Dr. Johan Wettergren for the productive collaboration, the discussions as well as the hospitality in RUAG. I would like to thank Prof. Lars Jonsson and Dr. Patrik Persson for the commitment to the project. I would like also to recognize the Onsala Space Observatory, Dr. Miroslav Pantaleev and Dr. Tobia Carozzi for the collaboration related to my department work.

I would like to thank to all my past and current colleagues in the Antenna Division and the Signal and Systems Department for the nice work environment. It has been a pleasure to share these years with such many friendly and interesting people. A special thanks goes to Madeleine, Aidin, Ahmed, Sadegh, Abbas, Jinlin, Oleg and Astrid. We had many good laughs, both in and out of work, thank you so much.

A special thanks to my friends here in Sweden, in particular Gabriel, Victor, Katharina, Livia, Rossella, Rocco and Giuseppe. Thank you for everything, you have been my family here is Sweden.

I would also like to thank my friends in Italy, especially Diana and Vittorio, for making me feel home regardless of the distance.

Finally my family: Mamma, papà, nicco e nonna, siete la mia vita.

Carlo
Göteborg, May 2015

List of Publications

This thesis is based on the following appended papers:

Paper 1
C. Bencivenni, M. Ivashina, and R. Maaskant, "A Simple Method for Optimal Antenna Array Thinning using a Broadside MaxGain Beamformer" *Eucap 2013, European Conference on Antennas and Propagation*, 8-12 April, Gothenburg, Sweden.

Paper 2
C. Bencivenni, M. Ivashina, R. Maaskant, and J. Wettergren, "Design of Maximally Sparse Arrays in the Presence of Mutual Coupling", in *IEEE Antennas and Wireless Propagation Letters*, Vol 14, pp. 159-162, 2015.

Paper 3
R. Maaskant, C. Bencivenni, and M. Ivashina, "Characteristic Basis Function Analysis of Large Aperture-Fed Antenna Arrays", in *Eucap 2014, European Conference on Antennas and Propagation*, 6-11 April, The Hague, the Netherlands.

Paper 4
C. Bencivenni, M. Ivashina, R. Maaskant, and J. Wettergren, "Fast Synthesis of Wide-Scan-Angle Maximally Sparse Array Antennas Using Compressive-Sensing and Full-Wave EM-analysis", submitted to *IEEE Transactions on Antennas and Propagation*, April 2015.

Other related publications by the Author not included in this thesis:

- R. Haas, M. Pantaleev, L. Helldner, B. Billade, M. Ivashina, O. Iupikov, C. Bencivenni, J. Yang, P. Kildal, T. Ekebrand, J. Jönsson, Y. Karandikar, and A. Emrich, "Broadband feeds for VGOS", *IVS 2014, International VLBI Service for Geodesy and Astrometry (IVS) General Meeting*, 2-7 March, Shanghai, China.

- M. Ivashina, T.S. Beukman, C. Bencivenni, O. Iupikov, R. Maaskant, P. Meyer, and M. Pantaleev, "Design of Wideband Quadruple-Ridged Flared Horn Feeds for Future Radio Telescopes", *Swedish Microwave Days*, 11-12 March, Gothenburg, Sweden.

- C. Bencivenni, M. Ivashina, and R. Maaskant, "Aperiodic Array Antennas for Future Satellite Systems", *Swedish Microwave Days*, 11-12 March, Gothenburg, Sweden.

- T. Beukman, M. Ivashina, R. Maaskant, P. Meyer, and C. Bencivenni, "A Quadraxial Feed for Ultra-Wide Bandwidth Quadruple-Ridged Flared Horn Antennas", *Eucap 2014, European Conference on Antennas and Propagation*, 6-11 April, the Hague, The Netherlands.

- M. Ivashina, C. Bencivenni, O. Iupikov, and J. Yang "Optimization of the 0.35-1.05 GHz Quad-Ridged Flared Horn and Eleven Feeds for the Square Kilometer Array Baseline Design", *ICEAA 2014, International Conference on Electromagnetics in Advanced Applications*, 3-9 August, Palm Beach, Aruba.

- M. Ivashina, R. Bradley, R. Gawande, M. Pantaleev, B. Klein, J. Yang, and C. Bencivenni, "System noise performance of ultra-wideband feeds for future radio telescopes: Conical-Sinuous Antenna and Eleven Antenna", *URSI GASS 2014, General Assembly and Scientific Symposium of the International Union of Radio Science*, 17-23 August, Beijing, China.

Acronyms

AESA	Active Electronically Scanned Arrays
CBFM	Characteristic Basis Functions Method
CS	Compressive Sensing
DRA	Direct Radiating Array
EEP	Embedded Element Pattern
EM	Electro Magnetic
GA	Genetic Algorithm
GO	Global Optimization
IEP	Isolated Element Pattern
MC	Mutual Coupling
MoM	Method of Moments
MSA	Maximally Sparse Array
SATCOM	Satellite Communication
SLL	Side Lobe Level

Contents

II Included Papers

Part I

Introductory Chapters

Chapter 1

Introduction

An array of antennas is a group of coordinated antennas designed to achieve improved performances and capabilities over a single-element antenna. Most notably, by deploying a number of antennas one can create directive and narrow beams or, in general, synthesize radiation patterns of arbitrary shape. Arrays also offer additional interesting capabilities such as electronic beam scanning, element redundancy and diversity.

These features are very attractive, especially for modern antenna systems, where reconfigurability and reliability are of key importance. However, the associated costs have thus far been prohibitive, limiting full-fledged arrays to few applications. Recent advances in manufacturing and electronics has rendered the array architecture appealing to a number of new applications. Today, there is a great interest in advanced array systems where major attention is paid to the main cost drivers as well as several practical design considerations. The objective is to minimize the total system cost and improve the maturity of array solutions in order to make them competitive against well-established technologies.

This thesis attempts to address some of these aspects and, in general, aims at improving state-of-art synthesis techniques with the focus on minimizing the array cost and improve the antenna system by introducing practical aspects early in the design phase. The work of this thesis is intended to be of general applicability, however particular attention has been given to satellite communication applications. Accordingly, most of the results and design aspects discussed throughout this thesis are demonstrated for such a scenario. The choice of application is motivated by the industrial partnership with RUAG Space AB as well as the challenging nature of designing antennas for such applications.

In the following subsection the considered satellite application and its technical specifications are introduced. In the remainder of this chapter the aims and the outline of the thesis are presented.

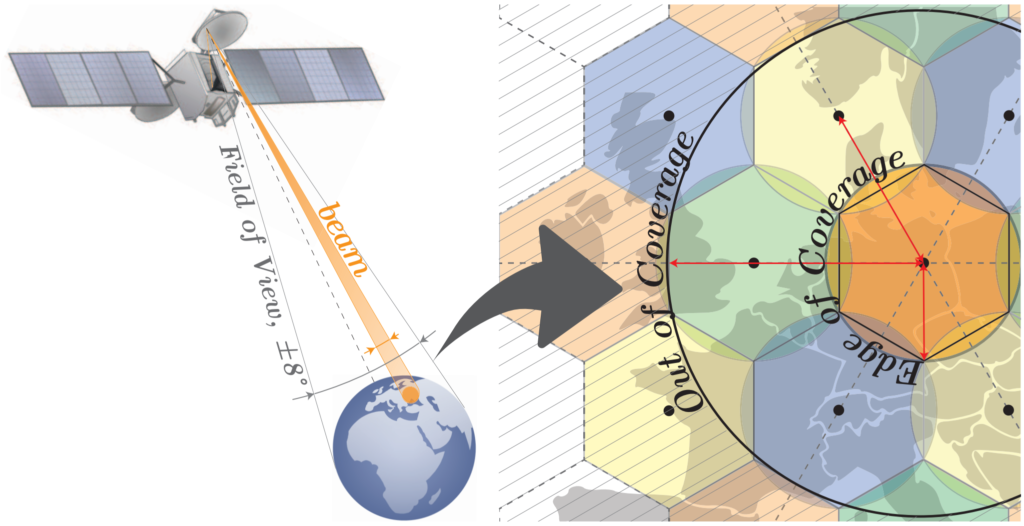

Figure 1.1: Illustration of a typical multi-spot GEO SATCOM scenario. The satellite illuminates Earth by means of beams (left). A hexagonal cell division with a 4-band reuse scheme (shown in color) is adopted (right).

1.1 SATCOM Applications

One of the foreseen applications for the next generation array antennas are Satellite Communication (SATCOM) [1]. In such a scenario, the onboard satellite antennas are designed to provide connectivity (Internet, TV and radio) to terminals located on the ground, see Fig. 1.1.

Current satellite systems typically deploy large reflectors with cluster feeds in a *one feed per beam* configuration. The increasing complexity due to multi-beam, multi-channel, dual-polarization and reconfigurability capabilities make such systems challenging in their design. A common view is that active arrays, also referred to as Direct Radiating Arrays (DRA:s), have the potential to handle such challenges and will have a leading role [2]. However, as of today, DRA:s are very expensive, mostly due to the high number of elements and associated electronic components. An example of two dense DRA:s of patch excited antennas for Medium Earth Orbit (MEO) communication at S-band are shown in Fig. 1.2. Geostationary Earth Orbit (GEO) antennas at K-band have about the same physical dimensions but larger electrical dimensions. Densely filled arrays for such applications are estimated to require a number of elements in the order of a thousand. Hence, there exists a strong interest in investigating new ways to design such arrays and to minimize the number of elements. For GEO satellites, the Earth is observable within an angular range of ±8°, often referred as Field of View (FoV), c.f. Fig. 1.1. Radiation outside this, i.e., towards open

Figure 1.2: Two dense DRA:s of patch-excited antennas for MEO communication at S-band. For GEO applications, an order of a thousands elements is expected.

Space, is lost power. However this is of minor concern since it does not lead to interference or a significant noise increase. To increase the system communication capacity, multi-beam strategies are employed. In a multi-beam spot configuration, pencil beams of about $0.5°$ to $1°$ in beamwidth provide a cellular-like hexagonal grid coverage with a 4-band frequency reuse scheme to isolate adjacent beams. To obtain such narrow beams, massive aperture diameters of about 100λ are required.

The most challenging aspect of these systems is to synthesize narrow beams with stringent interference levels over the entire FoV, see Fig. 1.1. The Edge of Coverage (EoC) of a beam is defined as the largest angular distance belonging to a cell (and beam): for a hexagonal grid this corresponds to the inter-beam distance divided by $\sqrt{3}$. Within this angular range, a maximum roll-off gain at the EoC is generally required so as to guarantee appropriate connectivity over the entire cell. The Out of Coverage (OoC) is the angular distance where the first iso-frequency interfering beam appears: for a 4-band system this amounts to 1.5 inter-beams. To respect the iso-frequency interference limits, very stringent Side Lobe Levels (SLLs) are required from the OoC to the FoV angle. Accordingly, the required radiation profile of the beam, called radiation mask, describes a minimum gain from broadside to EoC and a maximum SLL from the OoC to the edge of the FoV.

The considered case study is a K-band GEO SATCOM application, c.f. Table 1.1. Accordingly, beams should be optimized for an OoC angle of $\pm 0.795°$ and a maximum SLL of -25 dB. The array element type has been provided by RUAG Space AB [3] and is shown in Fig. 1.3. The array element is a circular corrugated pipe horn with an aperture diameter of 1.5λ. Over the FoV this element has a virtually constant directivity of about 9 dBi and a relative cross-polarization level in the order of -35 dB in the diagonal

Table 1.1: Specifications for the considered SATCOM application

Array type	Planar, dual polarized at K-band
Antenna Element type	Corrugated pipe horn by RUAG
Field of View (FoV)	$\pm 8°$
Beam arrangement	Multi-spot, 4-band hexagonal grid
Interbeam distance	$1.06°$
Edge of Cover (EoC) angle	$0.61°$
Out of Cover (OoC) angle	$0.795°$
Max. SLL in the OoC region	-25 dB

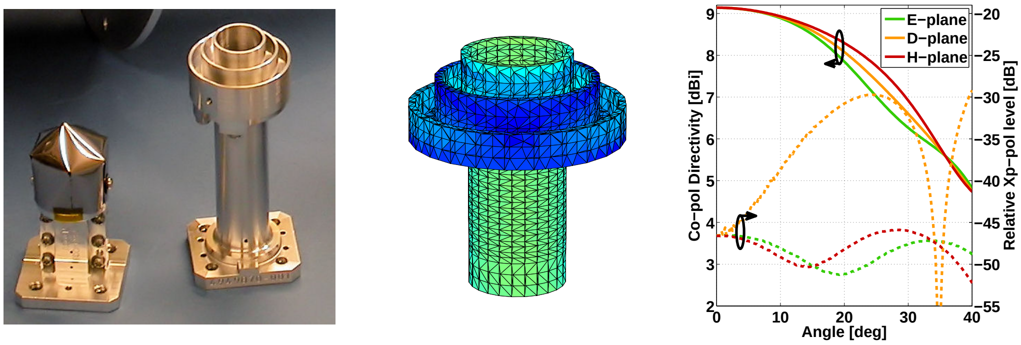

Figure 1.3: Corrugated pipe horn antenna element as designed by RUAG: manufactured (left), meshed MoM model and current distribution when excited by an internal monople (center), isolated element pattern (right).

plane, see Fig. 1.3 (right).

The very large array sizes and strict SLL specifications required in SATCOM applications make them very challenging in their design and therefore represents an interesting test bed for the method presented in this thesis.

1.2 Aim of the Thesis

The aim of this thesis is to investigate a new deterministic synthesis method for the design of aperiodic arrays, capable of modeling realistic EM effects of complex antennas as well as satisfying a number of performance requirements.

The main objective of the proposed method is to overcome the limitations of current synthesis techniques, which are either computationally intractable or employ too simplistic antenna models and specifications. To address the need for flexibility and computational efficiency we propose a deterministic approach based on Compressive Sensing theory. The problem is formulated in an iterative convex form which is solved efficiently and can be extended to include additional specifications in a straightforward manner.

One of the aims of the proposed method is to account for realistic antenna elements including mutual coupling effects, which are typically ignored in other synthesis methods. To address this, we propose an iterative full-wave hybrid approach, which starts from the array designed in the absence of mutual coupling effects and progressively refines the layout through an EM analysis. Additionally, we aim at designing arrays that behave well when scanning. For this purpose, the method has been extended to multi-beam optimization, mitigating scanning degradation due to beam deformation, quantized phase shifters and mutual coupling effects.

A very important aspect in reducing the manufacturing cost is to favor modular designs and component reuse. This objective has been investigated by imposing symmetric layouts and excitations. The formulation is kept general in the sense that it enables designers to enforce the desired symmetry type and its order for their application.

1.3 Thesis Outline

This thesis is subdivided into two main parts. The first part is organized in seven chapters and introduces the reader to the research topics as well as the main aspects of this work and ends with a concluding chapter. In the second part of the thesis, the author's most relevant contributions to the literature are included in the form of appended papers. Additional non-appended publications can be found as references in the section List of Publications.

In Chapter 2 the reader is provided with some theoretical background on arrays as well as to the problem of aperiodic array design and earlier work on the topic. This clarifies the context of the present research. In Chapter 3 the theoretical formulation utilizing Compressive Sensing theory is presented in relation to the aperiodic array synthesis problem at hand. Chapter 4 introduces mutual coupling effects, their modeling and the proposed hybridization of the method in order to include them in the design. In Chapter 5 the problem of multi-beam optimization for phase scanning applications is presented and formulated. The layout and excitations symmetries are investigated in Chapter 6 as a means to simplify the array layout and associated cost. Chapter 7 concludes the first part of the thesis with a brief summary of the main contributions and future work.

Chapter 2

Background on Antenna Arrays

An array of antennas is a set of antennas designed such that their combined output signals have desired EM filter characteristics in space. Arrays appear in very different forms: from a simple slotted waveguide to a complex network of antennas deployed over a large area.

Although arrays can have very different architectures, capabilities, specifications as well as challenges, the underlying operating principle is the same. Two main parts are identifiable: the first are the antenna elements, which are physically displaced over an area in order to realize an equivalent aperture distribution. The second part is the beamforming network, which is responsible for feeding or combining the element signals such as to obtain the desired beam characteristics.

In this chapter we first introduce the theoretical basis on array antennas. Classical regular arrays are also introduced so as to explain the limitations of regular arrays and classical analysis. Aperiodic arrays and Maximally Sparse Arrays are then presented together with a brief review on the research on these topics. The primary objective of this chapter is to introduce the reader to the context of this work.

2.1 Theoretical Basis

Consider N antennas placed at the locations $\{\boldsymbol{r}_n\}_{n=1}^N$ and the set of respective far-field vector element patterns $\{\boldsymbol{f}_n(\hat{\boldsymbol{r}})\}_{n=1}^N$, where the direction $\hat{\boldsymbol{r}}(\theta,\phi) = \sin(\theta)\cos(\phi)\hat{\boldsymbol{x}} + \sin(\theta)\sin(\phi)\hat{\boldsymbol{y}} + \cos(\theta)\hat{\boldsymbol{z}}$ (see also Fig. 2.1). The array far-field function can then be written as

$$\boldsymbol{f}(\hat{\boldsymbol{r}}) = \sum_{n=1}^{N} w_n \boldsymbol{f}_n(\hat{\boldsymbol{r}}) \quad \text{with} \quad \boldsymbol{f}_n(\hat{\boldsymbol{r}}) = \boldsymbol{f}_n^o(\hat{\boldsymbol{r}}) e^{jk\boldsymbol{r}_n\cdot\hat{\boldsymbol{r}}}, \tag{2.1}$$

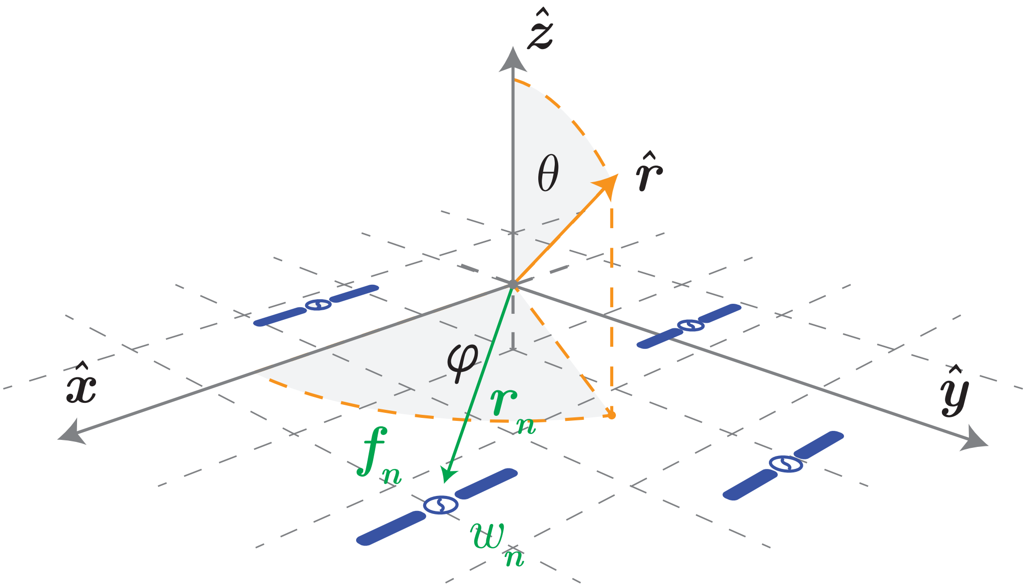

Figure 2.1: Illustration of a generic array layout; each antenna element is characterized by its position $\boldsymbol{r}_n$, embedded element pattern $\boldsymbol{f}_n$, and excitation coefficient w_n.

where w_n is the complex excitation coefficient of the nth element, and $k = 2\pi/\lambda$ is the wavenumber, respectively. Note that $\boldsymbol{f}_n$ includes the propagation phase delay with respect to $\boldsymbol{f}_n^o$, whose origin is on the element itself.

Now, for convenience, the vectorial form of the above expressions are also introduced. Let the N-dimensional excitation vector $\mathbf{w} = [w_1, w_2, \ldots, w_N]^T$, where ^{T} denotes the transpose, and let us expand $\boldsymbol{f} = f_{\text{co}}\hat{\mathbf{co}} + f_{\text{xp}}\hat{\mathbf{xp}}$ into its far-field co-polar and cross-polar components, respectively, then Eq. (2.1) can be rewritten in the compact form

$$\boldsymbol{f}(\hat{\boldsymbol{r}}) = [\mathbf{w}^T\mathbf{f}_{\text{co}}(\hat{\boldsymbol{r}})]\hat{\mathbf{co}} + [\mathbf{w}^T\mathbf{f}_{\text{xp}}(\hat{\boldsymbol{r}})]\hat{\mathbf{xp}}, \tag{2.2}$$

where $\mathbf{f}_\nu = [f_{\nu,1}, f_{\nu,2}, \ldots f_{\nu,N}]^T$ is an N-element column vector with $\nu \in \{\text{co}, \text{xp}\}$.

With reference to Eq. (2.1), the resulting far-field pattern is determined by the element patterns, positions and excitation coefficients. The first two quantities are defined by the physical geometry of the array and therefore are fixed once chosen. The excitation coefficients, on the other hand, can in principle be modified electronically, allowing to change the array pattern without any mechanical movement, see Chapter 5 for further details.

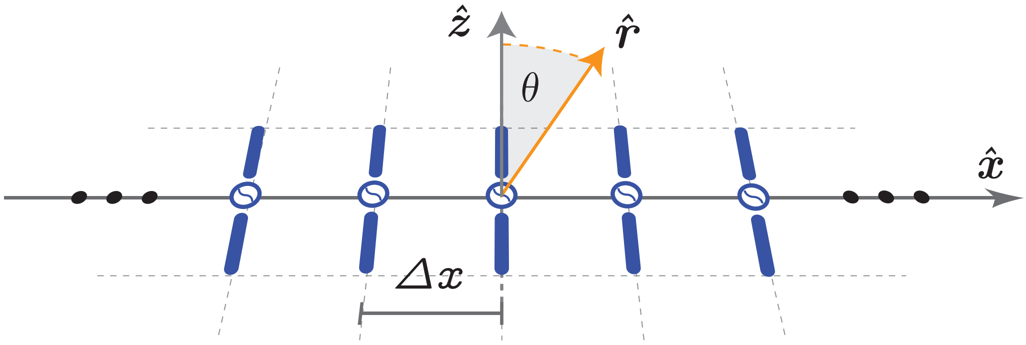

Figure 2.2: Illustration of a regular linear array; elements are placed along the x-axis with a constant inter-element distance Δx.

2.2 Array Factor and Regular Arrays

Most commonly arrays are assumed to have *equal* element patterns, i.e., all element patterns have the same shape and only differ by a phase and amplitude coefficient. Although this is generally not true due to the Mutual Coupling, as discussed in Chapter 4, this assumption greatly simplifies the design and the analysis of the array. Under such condition, we can factorize the far-field in (2.1) as

$$\boldsymbol{f}(\hat{\boldsymbol{r}}) = \boldsymbol{f}_0^o(\hat{\boldsymbol{r}})F(\hat{\boldsymbol{r}}) \quad \text{with} \quad F(\hat{\boldsymbol{r}}) = \sum_{n=1}^{N} w_n e^{jk\boldsymbol{r}_n\cdot\hat{\boldsymbol{r}}}, \tag{2.3}$$

where $F(\hat{\boldsymbol{r}})$ is the scalar Array Factor (AF) and $\boldsymbol{f}_0^o(\hat{\boldsymbol{r}})$ is the common vector element pattern centered at the origin. Accordingly, the element pattern defines the envelope of the far-field pattern. Once this is chosen, the design of the array reduces to the synthesis of the scalar AF. For the above expression to be valid, the common element pattern should be an acceptable approximation of the actual element patterns. This is true for weakly coupled antenna elements and for sufficiently large regular arrays, where in the former the Mutual Coupling is ignored while is included in the latter.

Regular arrays are an important class of array layouts where the element inter-distance is fixed and equal. The environment for every element except for those near the periphery is identical and equal to a that of an infinitely long regular array. For sufficiently large regular arrays, this element pattern representation (which includes the Mutual Coupling) is accurate enough since the effects due to the edge elements are limited.

Let us consider a regular linear array along the x-axis for simplicity as show in Fig 2.2. Accordingly, the AF in (2.3) can the be written as

$$F(\theta) = \sum_{n=1}^{N} w_n e^{jk(n\Delta x)\sin\theta}. \tag{2.4}$$

In a regular array, the layout is defined by the array aperture area A (or diameter D) and the inter-element spacing Δx. The former is directly related to the maximum array gain ($G = 4\pi A/\lambda^2$) and the corresponding minimum beamwidth [$\theta_{\text{HPBW}} = \arcsin(0.2572\lambda/D)$]. The second must be chosen small enough in order to guarantee the absence of grating lobes (see Chapter 3) in the visible range and, as such, is dependent on the scanning requirements. Spacings from $\lambda/2$ to λ guarantee the absence of grating lobes in the entire angular range depending on the scanning requirements. Accordingly, given the specifications for a regular array, the number of elements is readily determined.

The only remaining unknown, i.e., the element excitations, are then chosen depending on the desired pattern shape. Well-known closed-form solutions exist for the design of optimal excitations. Additionally, and as shown in Eq. (2.4), the far-field pattern and the element weights have a linear relationship, so that relatively straightforward beamforming algorithms can be applied to achieve desired patterns.

Regular arrays have the important advantage that they are accompanied by a set of well-established design rules, making them most popular.

2.3 Aperiodic Arrays

Aperiodic arrays are non-uniform arrays where the inter-element distances are not equal. First investigated by Unz [4], it was found that by tuning the element positions one is able to reduce the element number and/or sidelobe levels (SLL) relative to classical regular arrays.

Aperiodic arrays aim at reducing the number of elements by breaking the periodicity of regular arrays while increasing the element spacings. Equivalently, it means that by exploiting the additional degrees of freedom of the element positions it is possible to reduce the total number of elements.

Many approaches have been proposed for the synthesis of aperiodic arrays, from analytical methods to local refinement schemes. Unfortunately, the problem of synthesizing a Maximally Sparse Array (MSA), i.e., an array with the least number of elements, is very challenging. As expressed by (2.1), the relation between the array pattern and the element positions is given though the exponential function with a complex-valued argument, and is therefore highly non-linear and oscillating. Additionally, the infinite array approach cannot be applied to aperiodic arrays, so that most of the synthesis methods are limited to the case of isolated elements.

Typically, two broad classes of design methods can be identified: in *Sparse* arrays the elements are positioned according to some strategy; in *Thinned* arrays, starting from a filled regular array, elements are removed to obtain an aperiodic layout. For both classes of arrays, different techniques have been proposed. Below we provide a brief review of some of the most popular methods.

Global optimization techniques

Global Optimization (GO) techniques, and more generally, stochastic methods, are very popular in the design of aperiodic arrays. The first encouraging results were obtained in the 90s, when Haupt first applied GO methods to the synthesis of thinned arrays [5]. A number of techniques have been borrowed from the mathematics science field, refined, and subsequently been applied to the synthesis of aperiodic arrays. Some of the most popular GO methods are Genetic Algorithms [5], Particle Swarm [6], Ant Colony [7] and Invasive Weed Optimization [8]. GO techniques have been mostly applied to array thinning problems and in a few cases to synthesize sparse antenna arrays.

One of the most attractive aspect of GO methods is their flexibility. In general, it is possible to incorporate complex specifications in a heuristic fitness function and to include various additional aspects of interest owing to the generic trial and error nature of the approach.

The major limitation of such methods is their high computational complexity. In most cases, only small to medium sized problems are tractable but even these are often very time consuming to solve. For larger problems, their use is limited only to the refinement of an initial solution [9].

Analytical techniques

Several analytical techniques, and more generally, deterministic techniques, have been proposed for the synthesis of both sparse and thinned aperiodic arrays. In the 60s and 70s a large number of deterministic thinning algorithms were proposed [10–13]. However, due to the limited success in controlling the sidelobes, some researchers conjectured that *cut-and-try random placement* to be as effective as any deterministic placement algorithm could ever be [14].

Today, a number of effective deterministic techniques are available. Some worth mentioning are the Matrix Pencil Method [15], Almost Different Sets [16], the Auxiliary Array Factor [17], Poisson Sum Formula [18] and the Iterative Fourier Technique [19]. An interesting and intuitively simple method interprets the aperiodic problem as the discrete approximation of an optimal contiguous aperture taper distribution. Starting from a standard amplitude taper such as the Taylor [20] distribution, elements are placed with a density proportional to such distribution.

Analytical techniques can handle much larger problems and the solutions typically show a simpler relationship between the specifications and the array design as opposed to Global optimization methods, thereby helping designers to understand the relationship between the technical specifications and the synthesized solution. However, the major limitations are dictated by the rather simplified model and specifications they assume. Specifically, and in relation to the novel contribution discussed in this work, virtually no deterministic method accounts for mutual coupling effects. Additionally, and to the best of the author's knowledge, multi-spot optimization is often not addressed either.

2.4 Summary and Conclusions

This chapter has introduced the theoretical background on antenna arrays. Regular arrays were then briefly introduced to illustrate the limitations and assumptions of classical arrays. Aperiodic arrays were presented as a solution to further improve and optimize classical regular arrays. A short overview of aperiodic array synthesis techniques and their limitations was also given.

Aperiodic arrays are attractive since they reduce the number of elements with respect to classical regular arrays. Unfortunately, the synthesis of Maximally Sparse Arrays (the array with the least number of antenna elements) is very challenging. Current synthesis techniques are either limited to the use of simplified models and specifications (analytical methods) or have prohibitive computational requirements (global optimization methods). For these reasons, there is a strong interest in a new aperiodic array synthesis technique which is both effective and flexible enough to be used for more practical designs.

Chapter 3

Compressive Sensing for Aperiodic Array Design

Compressive Sensing (CS) is a Signal Processing technique designed for the efficient sampling and reconstruction of a continuous signal [21]. In fact, by exploiting the natural sparsity of a continuous signal it is possible to greatly reduce the number of samples required to reconstruct the signal with respect to the classical Nyquist–Shannon sampling criterion.

A parallel can be drawn with the Maximally Sparse Array (MSA) synthesis problem. In the antenna scenario, the problem is to minimize the number of spatial samples (antenna elements) required to synthesize a desired radiation pattern [22]. The parallel between the two problems is further clarified by the relationship between the Fourier Transform of the (sampled) time signal in the Signal Processing case and the Array Factor of the (sampled) aperture field distribution in the array case.

The CS problem is then solved in an approximate form through an iterative weighted ℓ_1-norm minimization procedure [23]. This formulation allows for an efficient and deterministic solution by means of standard convex optimization algorithms. Furthermore, the algorithm is flexible enough to include additional constraints, provided they can be expressed, or be approximated, in a convex form (more details in Sec. 3.3).

In this chapter we briefly introduce the theoretical basis behind Classical and CS sampling. Throughout this chapter the parallels between the Signal Processing and Aperiodic Array Synthesis techniques are illustrated. The weighted iterative convex ℓ_1-norm optimization formulation is introduced afterwards. The method is demonstrated for the synthesis of small aperiodic arrays of isotropic radiators.

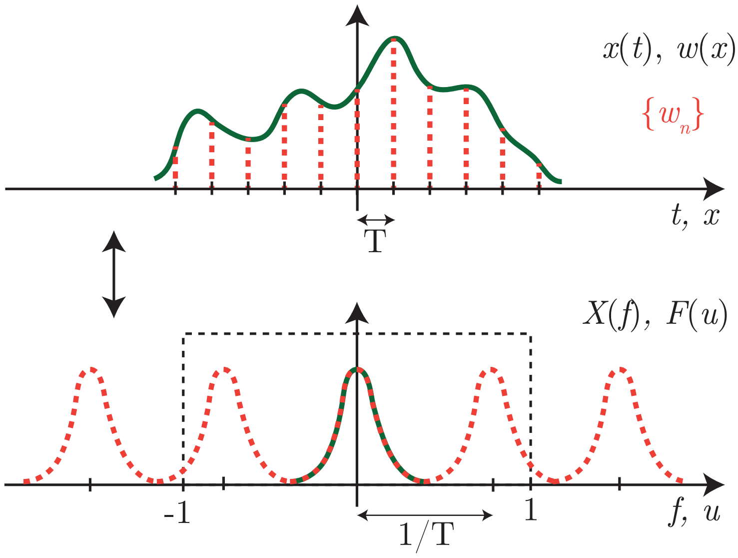

Figure 3.1: Illustration of the Nyquist sampling criterion/grating lobe free condition. In the time/space domain (top), the original continuous signal/aperture field distribution (in green) is sampled uniformly with T step (red). In the transformed frequency/array factor domain (bottom), the sampled signal (red) is a series of displaced replicas of the continuous signal (green) with period $1/T$. In arrays, the visible range extends from $u \in (-1, 1)$ (black).

3.1 Nyquist Sampling and Grating Lobes

The Nyquist–Shannon sampling criterion guarantees lossless reconstruction of a continuous signal when uniformly sampling at twice the maximum frequency of the original signal. However, the theorem does not preclude the reconstruction in circumstances that do not meet the sampling criterion.

Notice the parallel between the Discrete Time Fourier Transform (DTFT) and the Array Factor (AF) expression (2.4):

$$X(f) = \sum_{n=-\infty}^{\infty} x(nT)e^{-j2\pi fTn} \longleftrightarrow F(u) = \sum_{n=1}^{N} w\left(n\frac{\Delta x}{\lambda}\right)e^{j2\pi u\frac{\Delta x}{\lambda}n} \qquad (3.1)$$

where in the equation on the left, $x(t)$ is the continuous signal sampled with the period T and $X(f)$ is the DTFT, periodic with period $1/T$; in the equation on the right, $w(x)$ is the aperture field distribution sampled at uniform distance $\Delta x/\lambda$ and $F(u)$ is the AF, periodic with period $\lambda/\Delta x$. The AF is a function of $u = \sin\theta$, thus the *visible range* extends between $u = \pm 1$ ($\theta = \pm 90^o$). When the inter-element distance $\Delta x > \lambda$, replicas of the main beam will be visible, as shown in Fig. 3.1. These new lobes,

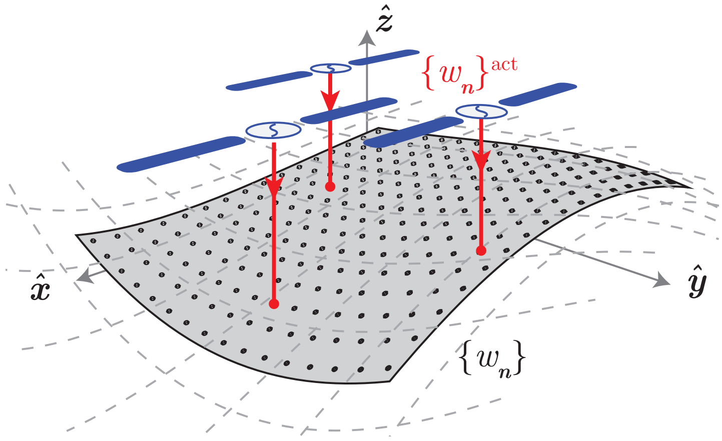

Figure 3.2: Illustration of a generic surface (gray) and its sampling (black dots). Between all the samples and the corresponding excitations $\{w_n\}$, only *active* samples (in red) are replaced by actual elements (in blue).

referred to as Grating Lobes, are highly undesired since they have the same amplitude of the main lobe (minus the attenuation effect due to the element pattern), thus compromising the directivity and dramatically increasing the SLL. When scanning up to the angle θ_s, the Grating Lobes free condition becomes roughly $\Delta x/\lambda \leq 1/(1 + |\cos\theta_s|)$ [24].

As a result, the arise of Grating lobes prevents from increasing the inter-element distance and reducing the number of elements in a periodic layout. Since this effect is due to the adopted periodicity of the element positions, choosing aperiodic layouts helps to reduce the effect of coherent field summation in unwanted directions.

3.2 Compressive Sensing Sampling

CS is a technique for minimizing the number of samples required to reconstruct a signal. Typically, signals are sampled according to the Nyquist criterion and are processed afterwards by a compression algorithm. CS, on the other hand, aims at directly minimizing the number of samples.

To find a minimal representation of the signal, CS relies on the solution of an under-determined system - a linear system of equations with more unknowns than equations. Under-determined systems have an infinite number of solutions, in order to choose one, additional constraints should be added. In compressive sensing the additional constraint is the sparsity condition which can be enforced by minimizing the number of non-zero components of the solution vector. In mathematical terms, the function returning the number of non-zero vector elements is the ℓ_0-norm.

In the array scenario, given an aperture sampling, the problem of designing a maximally sparse array is finding the excitation set $\{w_n\}$ with the minimum number of non-zero entries $\{w_n\}^{\text{act}}$ while fulfilling certain pattern constraints, as shown in Fig. 3.2. Using the vector notation introduced in Eq. (2.2), the optimization problem can be stated as finding $\mathbf{w} \in \mathbb{C}^N$ such that [23]

$$\underset{\mathbf{w}\in\mathbb{C}^N}{\operatorname{argmin}} \|\mathbf{w}\|_{\ell_0}, \text{ subject to a } \textit{set of constraints}. \tag{3.2}$$

For pencil beam synthesis and for a beam with a maximum co-polar directivity in the scanning direction $\hat{\boldsymbol{r}}_s$ and a radiation mask M_ν on the ν component of the field, the set of constraints can be written as

$$\textit{set of constraints}: \begin{cases} f_{\text{co}}(\hat{\boldsymbol{r}}_{\text{s}}) = 1, \\ |f_\nu(\hat{\boldsymbol{r}})|^2 \leq M_\nu(\hat{\boldsymbol{r}}), \hat{\boldsymbol{r}} \in \text{mask} \end{cases} \tag{3.3}$$

3.3 Iterative ℓ_1-norm Minimization

Unfortunately, Eq. (3.2) cannot be solved directly and finding a solution using a combinatorial search method is intractable, even for moderate array sizes [25]. More specifically, using arguments in the field of computational complexity theory, a problem is considered solvable if the solution time has a polynomial relationship with the problem size (Cobham's thesis). Therefore, problems whose solution can be found in polynomial time are called Polynomial (P) for short and are considered *easy* to solve. Nondeterministic Polynomial (NP) problems are the superclass of problems where verifying a hypothesis of the solution is polynomial (but solving is in general not). NP-hard problems are a separate class of problems which are defined to be at least as hard as the hardest problems in NP. That is, in practice, just verifying a solution hypothesis for such problems is already prohibitive. Eq. (3.2) can be shown to be an NP-hard problem [26], therefore solving the CS problem in a rigorous way is computationally infeasible.

To overcome this, approximate solution techniques are considered. In [23], the problem is relaxed and solved in a semi-analytical manner by approximating the ℓ_0-norm minimization through an iterative weighted ℓ_1-norm minimization procedure. One iteration of the algorithm reads [23]

$$\underset{\mathbf{w}^i\in\mathbb{C}^N}{\operatorname{argmin}} \|\mathbf{Z}^i\mathbf{w}^i\|_{\ell_1}, \text{ subject to a } \textit{set of constraints} \tag{3.4}$$

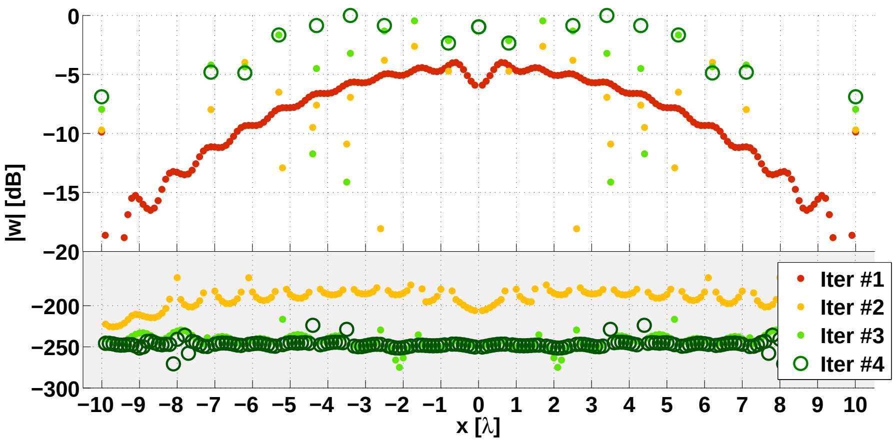

Figure 3.3: Excitation coefficient magnitudes for subsequent iterations.

where the m^{th} element of the diagonal matrix $\mathbf{Z}^i$ is given by,

$$z_m^i = \frac{1}{|w_m^{(i-1)}| + \epsilon}. \tag{3.5}$$

The matrix $\mathbf{Z}^i$ is chosen to maximally enhance the sparsity of the solution $\mathbf{w}^i$; that is, redundant elements are effectively suppressed through magnifying their apparent contribution in the minimization process by an amount that is based on the previous solution $\mathbf{w}^{(i-1)}$. The parameter ϵ enables elements that are "turned off" to be engaged again later on during the iterative procedure. It is recommended to set ϵ slightly smaller than the smallest expected active excitation for an optimal convergence rate and stability. Typically, this numerically efficient procedure requires only few iterations for the excitation vector to converge.

Both the minimization problem and the set of constraints are formulated in a convex form, so that standard convex programming algorithm can be used to find a solution in a deterministic manner. For a convex problem the local minimum coincides with the global one, so that the solution is easily found.

3.4 Results

The CS approach is here demonstrated in the synthesis of a linear symmetric array. To further illustrate the behavior of the method, the evolution of the synthesis process is examined. The chosen array is a linear array of isotropic radiators with an aperture diameter $d = 20\lambda$ and -20 dB SLL.

The aperture is first sampled finely so as to emulate a quasi-continuous element positioning (typical step size is $\Delta d = \lambda/100$, although here $\lambda/10$ is

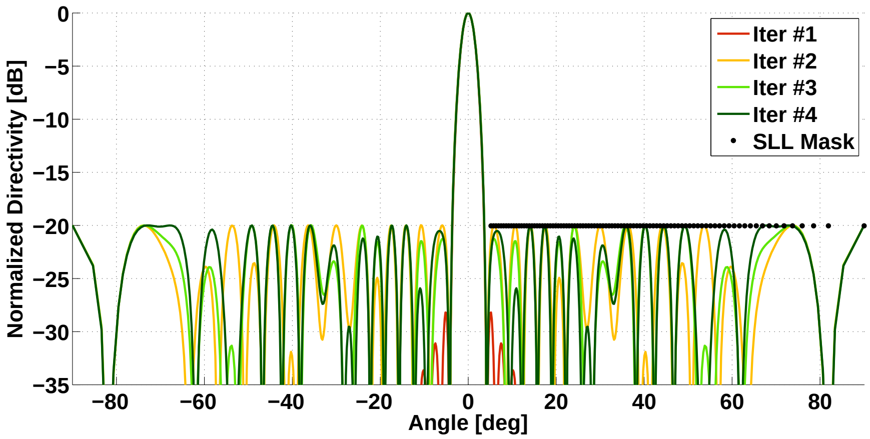

Figure 3.4: Far-field radiation pattern for subsequent iterations.

preferred for graphical reasons), and phase-shifted versions of the element pattern are assumed. The ℓ_1-norm minimization is then iterated until convergence of $\mathbf{w}$ occurs, yielding the optimal array layout. Although the optimization solution includes all the possible element positions, it is straightforward to identify active elements by a threshold level on the excitation magnitudes. Since, typically, inactive elements have normalized magnitudes in the order of -200 dB, the distinction is clear and their removal from the actual array has no practical impact on the final pattern.

In Fig. 3.3 the evolution of the element weights is shown, while the corresponding far-field patterns are illustrated in Fig. 3.4. In just 4 iterations the algorithm, starting from a quasi-continuous element distribution, selects only 17 active elements and the corresponding weights that guarantee the required far-field requirements. The remaining elements have weights between -200 dB and -300 dB in magnitude and will therefore not have a noticeable effect on the far-field pattern when removed.

3.5 Summary and Conclusions

In this chapter the Compressive Sensing approach was introduced and then applied to synthesize a Maximally Sparse Array antenna. Shannon's classical sampling criterion and the grating lobes-free condition were introduced to present the limitations of a regular sampling. The problem of Compressive Sensing was then formulated whose solution was approximated through an iterative convex minimization procedure. The approach was demonstrated in the design of linear aperiodic antenna arrays of isotropic elements.

The Compressive sensing approach has several interesting characteristics. The convex formulation allows for the problem to be solved in an efficient and deterministic manner. Additionally, it is flexible and can be supplemented by additional constraints when these are expressed in a convex form.

Chapter 4

Antenna Mutual Coupling

The antenna radiation characteristics are strongly influenced by the immediate environment, in particular by conducting bodies. In an array, the proximity between antenna elements can strongly affect their far-field patterns and impedance characteristics. This effect, known as Mutual Coupling (MC), is often undesired but can also be exploited to improve directivity and bandwidth.

As discussed in Chapter 2, in array analysis and design, it is common to assume *identical* element pattern shapes. This approximation is appropriate for weakly coupled antennas (where MC can be ignored) and large regular arrays (where the majority of the elements experience identical MC effects).

In aperiodic arrays, the irregular structure and the dense element clusters complicate the modeling as the element patterns can be very different from one another. The complexity of the MC effects and the lack of simple mathematical models require us to perform a time-consuming full-wave analysis. As a consequence, designing aperiodic arrays with MC included is practically impossible for analytic methods as well as computationally intractable for global optimization methods. For this reason, aperiodic array synthesis methods assume isolated element patterns, despite such approximation may not always be accurate.

The herein proposed CS method has been extended for the inclusion of MC effects in the synthesis of aperiodic arrays through an iterative full-wave analysis. The array is first designed by assuming Isolated Element Patterns, i.e., without MC effects, and simulated by the Method of Moment analysis to evaluate the effects of MC. The array is then iteratively refined using the Embedded Element Patterns that include the MC effects, until convergence is reached. The algorithm typically converges in few iterations making it numerically efficient.

In this chapter we describe the basic theory on MC effects and its inclusion in the array synthesis algorithm. Results are shown for the synthesis of

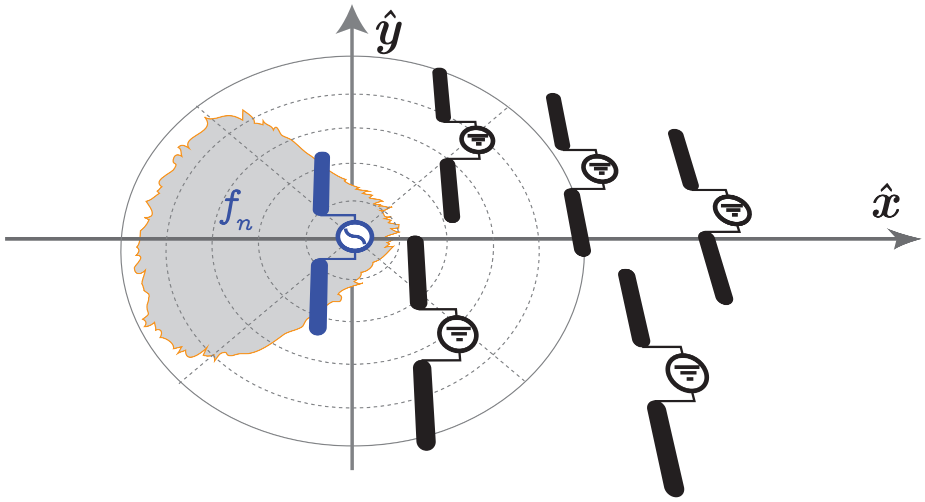

Figure 4.1: Illustration of the Embedded Element Pattern: the EEP $\boldsymbol{f}_n(\hat{\boldsymbol{r}})$ (gray) is defined when the element n is excited (blue) and the rest are passively matched terminated (black).

a linear array of highly coupled dipole antenna elements and a planar array of weakly coupled horns. Finally, a summary and the conclusions are given.

4.1 Embedded Element Pattern

Antennas are typically characterized in free space, i.e., in *isolation* from any other body, and are described by the Isolated Element Pattern (IEP). Once an antenna element is placed inside an array, the proximity to other elements will influence its behavior due to Mutual Coupling (MC). Exciting one antenna induces currents on nearby elements which can re-radiate and subsequently couple to other antennas. This gives rise to two effects: (i) a change in the total pattern due to radiating currents induced on the other antennas; (ii) a change in the antenna impedance due to the induced current at the antenna ports. These effects are dependent on the element excitations, or in the case of phased arrays, on the scanning direction. In practice, the magnitude of such effects is strongly affected by the element directivity and spacing. Due to a lack of simple mathematical models it is in general impossible to predict MC a priori.

A common approximation to the analysis of MC effects is the *isolated element approach* [24], where the shape of the electric current is assumed identical for all elements. This is valid only for single mode antennas, where the geometry of the antenna element supports only one current mode. For example, in the specific case of a minimum scattering antenna (e.g. halfwave dipoles), the neighboring antennas are effectively invisible when open-circuited. As a result, when the antennas are terminated, the resulting pattern of one excited antenna can be expressed as the sum of the identical patterns of all elements multiplied by their correspondingly induced currents. The inclusion of the MC effects therefore reduces to find the induced currents on neighbouring elements when one is excited, which can be done through the antenna input impedance matrix. The impendence matrix can be obtained by means of a full-wave analysis and can be used directly to compensate for MC effects [27].

The approach adopted here is the more general *embedded element approach* (in the past, the term active element has become disfavoured) [28]. The Embedded Element Pattern (EEP) is defined as the element pattern when one element is excited and the rest of the elements are passively terminated by a matched load, see Fig. 4.1. When this representation is adopted, Eq. (2.1) is valid since the MC effects are incorporated in the EEP definition. Additionally, this definition is not limited to single mode antennas, although still dependent on the choice of the antenna port termination. The excitation coefficients $\{w_n\}$ represent the incident voltage excitation and while the scan impedance can be calculated from the N-port S-parameters.

It is pointed out that, changing the element positions would modify the resulting mutual impedance and EEPs. Hence, regardless of the representation, the MC must be recalculated for a specific array layout.

4.2 Fast Array Simulation by CBFM

A full-wave analysis of electrically large structures is often resource demanding, which renders the analysis of arrays of complex antennas impractical. The Method of Moments (MoM) is a popular numerical method based on an integral formulation of the Maxwell equations. In MoM, the unknown current distribution $\boldsymbol{J}$ is discretized by dividing the antenna surface in N_J appropriately sized facets (the mesh) supporting the current basis functions as

$$\boldsymbol{J}(\boldsymbol{r}) = \sum_{n=1}^{N_\mathrm{J}} I_n \boldsymbol{J}_n(\boldsymbol{r}), \tag{4.1}$$

where $\boldsymbol{J}_n$ and I_n are the nth basis function and its unknown expansion coefficient, respectively. The unknown currents at the N_J basis function supports are solved by testing the boundary conditions using N_J test weight functions leading to a system of linear equations of the form

$$\mathbf{ZI} = \mathbf{V}, \tag{4.2}$$

where $\mathbf{I}$ is the vector of unknown expansion coefficients for the current, while $\mathbf{Z}$ and $\mathbf{V}$ are the moment matrix and excitation vector, respectively.

With reference to (4.2), storing the moment matrix requires $O(N_J^2)$ memory, while performing the matrix inversion requires $O(N_J^3)$ solve time. As example, a single pipe horn element (Section 1.1) requires about 9000 Rao-Wilton-Glisson basis functions. Consequently, only arrays of very few of these elements can be simulated in practice by standard MoM methods on regular computing platforms, while the desired array sizes that we need to consider can be in order of hundreds of elements.

The Characteristic Basis Function Method (CBFM) is a macro domain basis function method that greatly reduces the numerical complexity of the antenna array analysis [29]. The method first analyzes the characteristic behavior of the single antenna, then maps the Local Basis Functions to a restricted set of Characteristic Basis Functions on the whole antenna. The method compresses the number of unknowns that need to be solved for in (4.2) by assuming that only a reduced set of current distributions are sufficient to accurately represent the actual current distribution. The total current can therefore be represented as

$$\boldsymbol{J}(\boldsymbol{r}) = \sum_{c=1}^{N_{\mathrm{CBF}}} I_c^{\mathrm{CBF}} \boldsymbol{J}_c^{\mathrm{CBF}}(\boldsymbol{r}) \quad \text{with} \quad \boldsymbol{J}_{p,s}^{\mathrm{CBF}} = \sum_{n=1}^{N_{\mathrm{p}}} I_{n,p,s} \boldsymbol{J}_{n,p}(\boldsymbol{r}), \tag{4.3}$$

where $\boldsymbol{J}_{p,s}^{\mathrm{CBF}}$ is the sth CBF of the pth antenna. Eq. (4.2) can then be rewritten in terms of the above unknown CBF coefficients. Typically, starting from a very large number of local basis function, only a very reduced set of CBFs is sufficient for the accurate representation of the current distributions on the elements, therefore resulting in a very large compression (typically factor 100 in the number of unknowns) of the linear system of equations.

4.3 Inclusion of Mutual Coupling Effects

The proposed synthesis method involves two subsequent steps, as shown in Fig. 4.2 [30].

First, the MSA is designed in the *absence* of MC effects as in the previous chapter and in accordance with other aperiodic synthesis methods. For this *initial*, uncoupled array design, phase-shifted versions of the EM-simulated isolated element pattern (IEP) are assumed. The ℓ_1-norm minimization is invoked and the active elements are identified by thresholding on the excitation magnitudes.

In the second step, an iterative, full-wave optimization is performed where the ℓ_1-norm minimization approach is hybridized by a full-wave EM

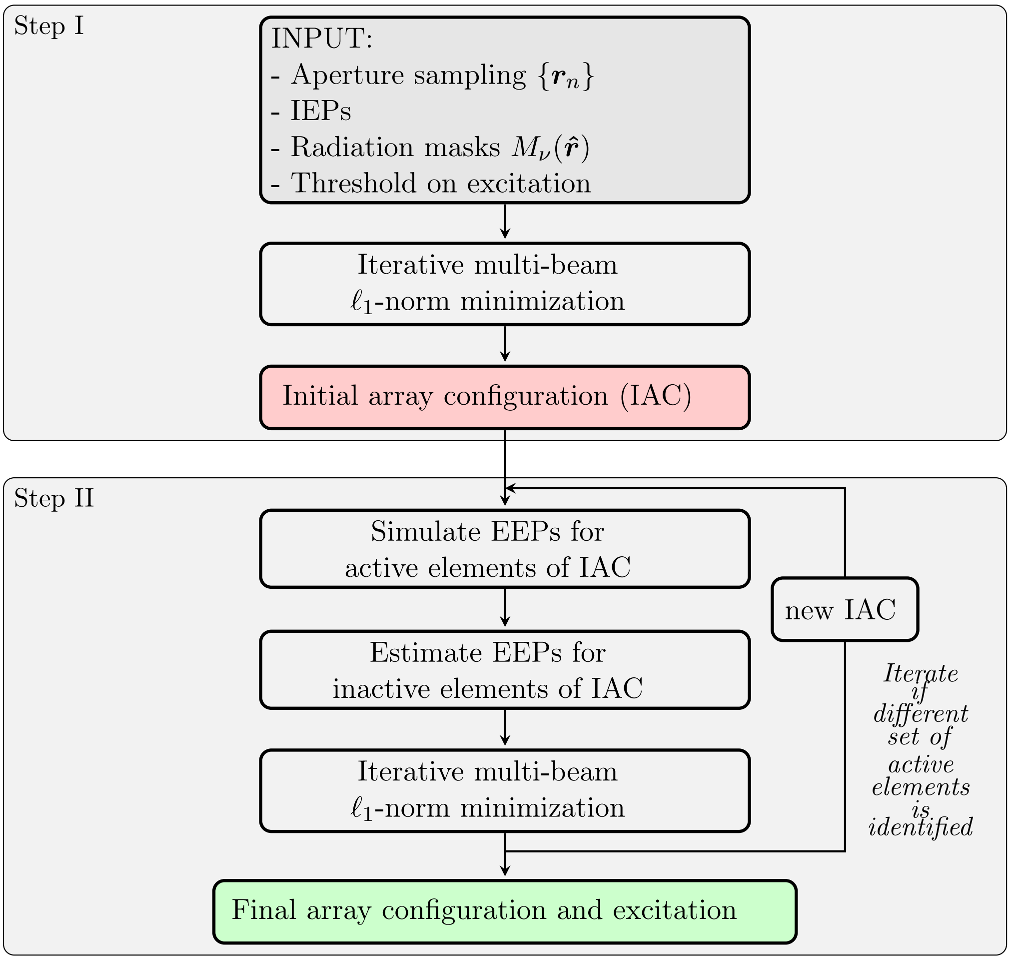

Figure 4.2: Block diagram of the proposed optimization approach, where IEP and EEP denote the isolated and embedded element patterns, respectively.

analysis. First, we perform a full-wave analysis of the active elements of the initial array layout to estimate the MC effects as well as to obtain the EEPs of the active elements. The isolated element patterns for the active element are then replaced by the simulated EEPs. The element patterns of the inactive elements are estimated by assuming a phase-shifted version of their nearest simulated EEP[1]. With this new set of EEPs, the ℓ_1-norm minimization algorithm is invoked again to obtain a new array layout. This procedure is repeated until the convergence criterion is satisfied, i.e., the state of active and inactive elements remains the same between two subsequent iterations. Typically, few MoM-ℓ_1 iterations are needed to reach convergence; for the MoM analysis, the full-wave in-house developed CAESAR solver is used [31]. Including the coupling effects in the synthesis phase does not only allow us to correct for the associated degradations, but also allows us to exploit such effects to improve the array design.

4.4 Results: Linear Array of Dipoles

The validity of the above extended method has been demonstrated in the synthesis of a small symmetric linear aperiodic array of parallel dipoles. We consider the problem of designing a broadside array of aperture size $d = 10\lambda$. The chosen SLL mask has the main lobe confined in the $|\theta| \leq 5.5°$ ($|u| \leq 0.0965$) region and a SLL of -22 dB. These specifications are chosen to be similar to those frequently used when benchmarking array synthesis algorithm, although a slightly more stringent SLL with respect to the typical -20 dB has been chosen to compensate for the slightly higher element directivity with respect to the commonly employed isotropic radiator. Furthermore, since we consider a broadside scanned array of identical antenna elements, a symmetric array layout will be synthesized.

As discussed, the array is first optimized assuming isolated element patterns. This initial design is then simulated by a full-wave analysis to asses the coupling effects. Fig. 4.3 shows the meshed model. The resulting normalized directivity when including MC effects, shown in Fig. 4.4, registers a SLL degradation of about 7 dB in proximity of the main lobe. Fig. 4.5 shows the IEP and EEPs for the positive x-positioned elements only, due to the symmetry.

Starting from this initial design, the algorithm proceeds to re-optimize the array excitations and layout for the updated set of EEPs. The evolution of the positive elements for each MoM-ℓ_1 iteration is summarized in Table 4.1. Fig. 4.6 shows the corresponding directivity patterns for each

[1] If needed, more sophisticated pattern interpolation techniques can be used to better estimate the embedded element patterns of inactive elements.

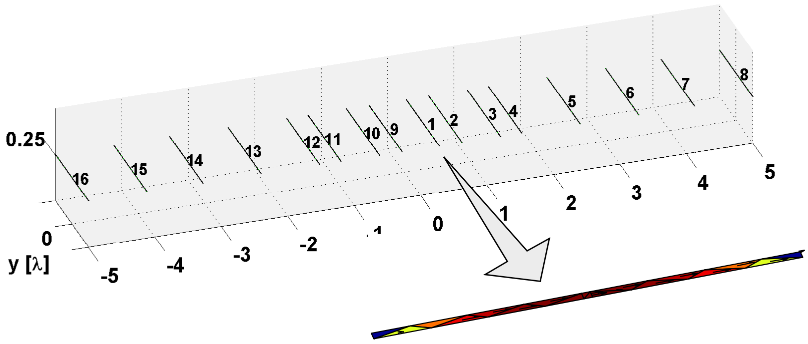

Figure 4.3: Perspective view of meshed geometry for the initial array and detail of the current distribution on one element.

iteration. The initial and final element positions and weight magnitudes are shown in Fig. 4.7, where one can observe how the central and dense part of the array layout changes upon introducing MC effects. The array layout converges in just 3 iterations, reduces the elements from 16 to 12 and corrects the SLL, while the broadside directivity is barely compromised.

4.5 Results: Planar Array for SATCOM

Mutual coupling effects are also shown for a SATCOM application scenario: the design considered is a 8-fold symmetric array optimized for full multi-beam applications, as further discussed in Section 5 and 6. The resulting array is a large planar array of 385 horn type antennas, its CBFM-model is shown in Fig. 4.8. The minimum inter-element distance varies between 2λ to 6.7λ with dense element clusters as well as sparsely spaced elements, therefore MC effects as well as strong variations between the element patterns are expected. As shown in Fig. 4.9, the EEPs exhibit a strong oscillating behaviour around the IEP (bold lines). The co-polarization component shows a ripple of about ± 2 dB and the cross-polarization about ± 20 dB around the IEP.

The total array patterns in the D-plane are shown in Fig. 4.10. The pattern computed from the initially assumed IEPs are compared to the MoM-simulated EEPs. The co-polarization component (left) has an increase in the SLL of about 1 dB both in the close proximity of the main beam as well as for far-off scanned beams. The cross-polarization pattern (right) is affected with an increase of about 10 dB in the broadside direction and around 30 dB over the rest of the FoV.

It is worth noticing that, despite the strong distortion of the EEPs, the effects on the total co-polar pattern are limited. As a result, the al-

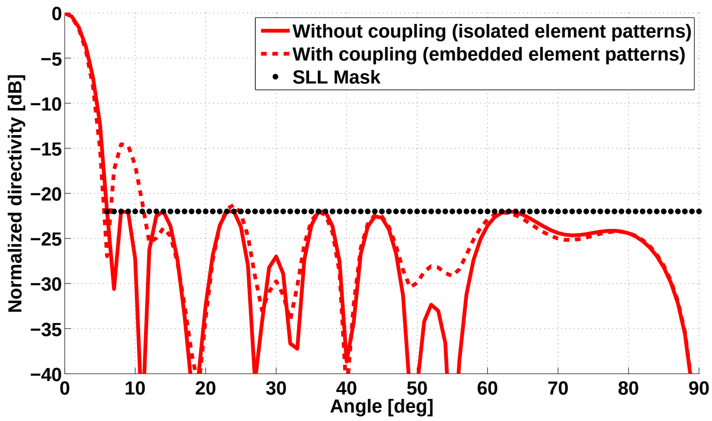

Figure 4.4: Normalized directivity with and w/o MC effects for the initial array.

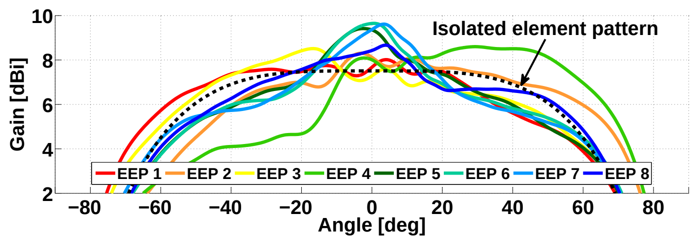

Figure 4.5: Isolated and embedded element patterns for terminated case (75Ω).

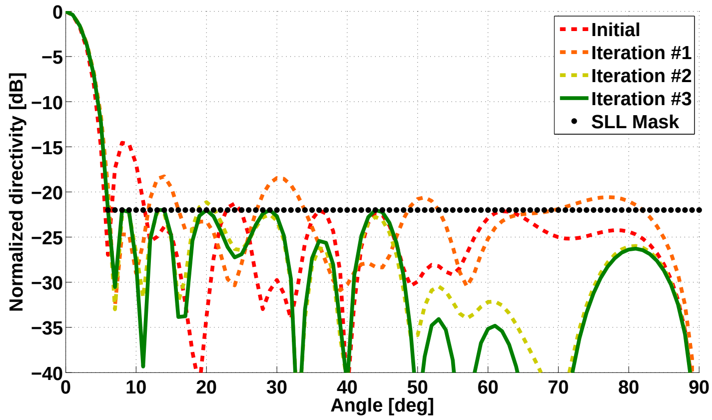

Figure 4.6: Normalized directivity in the presence of MC for subsequent iterations.

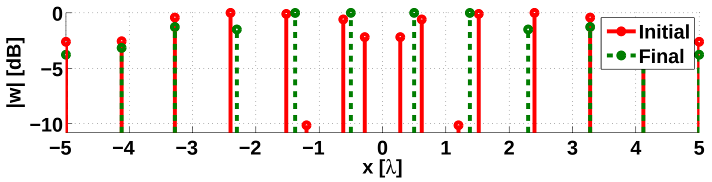

Figure 4.7: Active elements positions and weights magnitude of initial and final array. Inactive elements (not shown) have magnitudes smaller than -200 dB.

Iteration	1	2	3	4	5	6	7	8
Initial	0.28	0.62	1.2	1.52	2.4	3.28	4.12	5
Iter#1		0.5		1.38	2.4	3.28	4.12	5
Iter#2		0.5		1.38	2.3	3.28	4.12	5
Iter#3		0.5		1.38	2.3	3.28	4.12	5

Table 4.1: Element positions in wavelengths for each iteration

gorithm corrects for this distortion with just two additional iterations and without significantly modifying the array layout. On the other hand, the cross-polarization pattern modeled through the EM-analysis shows much higher levels than those predicted during the optimization procedure when ignoring MC effects, but are still acceptable for the chosen scenario. For applications that are more susceptible to cross-polarization variations or high cross-polarization levels it is recommended to include the cross-polar mask constraint levels in the optimization process.

4.6 Summary and Conclusions

In this chapter the problem of the aperiodic array synthesis in the presence of mutual coupling effects has been considered. Both analytical and global optimization algorithms often assume isolated element pattern due to the complexity of the MC effects in aperiodic lattices, but this represents not always an accurate assumption. The proposed synthesis method has been extended to include MC effects by adopting an iterative refinement approach involving rigorous EM-simulations. The method converges in few iterations with a limited computational burden [32].

The results have been demonstrated in the synthesis of a linear array of highly coupled dipole elements. The array design is improved with a reduction in the number of elements while being able to recover the strongly degraded side lobes back to the desired level. In the case of a planar array of horn type antennas it is shown that the changes in the co-polar levels are limited as opposed to the cross-polar levels.

The ability to include mutual coupling effects in the synthesis of aperiodic arrays has therefore shown to be critical in certain cases. In fact, by assuming isolated element pattern can be inadequate, especially in the case of a densely packed array of highly coupled antenna elements. Additionally, since the procedure is iterative in nature, the designer can decide to include the coupling correction only when needed.

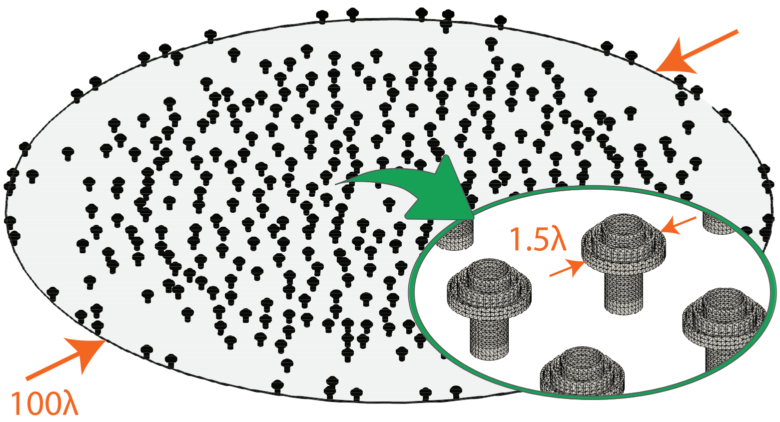

Figure 4.8: Array full-wave meshed model comprising 385 pipe horn antenna elements.

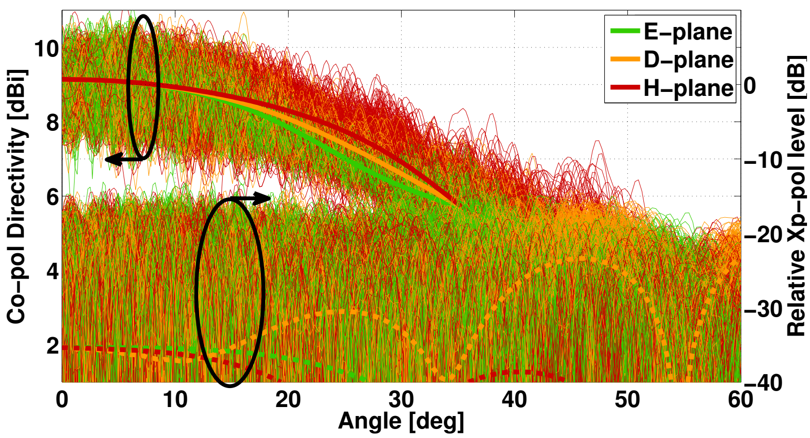

Figure 4.9: Simulated Embedded Element Patterns in comparison with the Isolated Element Pattern (bold line).

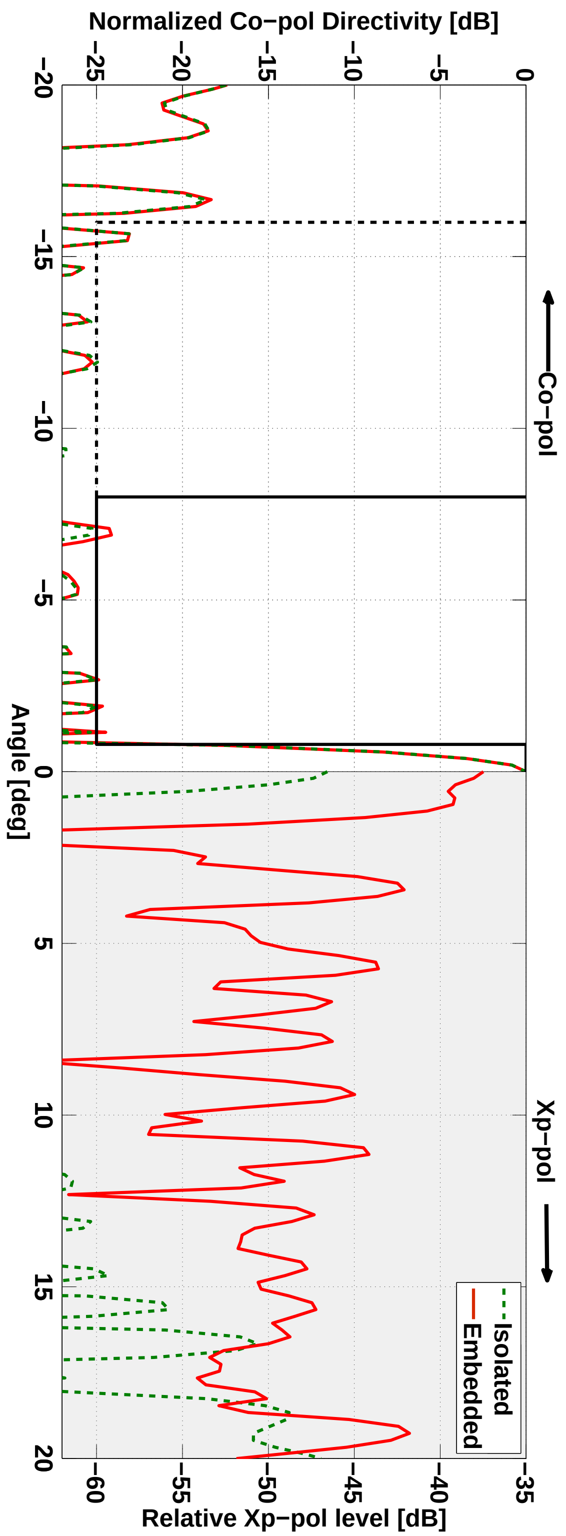

Figure 4.10: Far-field pattern without mutual coupling (isolated element pattern) and after full-wave analysis (embedded element patterns).

Chapter 5

Multi-beam Optimization

One of the array's most attractive features is the ability to modify the radiation pattern electronically. By changing the set of complex element excitations it is possible to switch between different beams, without any mechanical action on the antenna. In phase scanned arrays multi-beam capabilities are obtained by phase control only. The array is designed for a specific beam shape, commonly a pencil beam, which can be re-directed (scanned) by changing the element excitation phases. Since the amplitudes are kept constant, only a time delay (or phase shifter) is needed at each element. Phased arrays can benefit significantly from cost reduction, beam-forming network simplification, and a constant amplifier efficiency.

Phased arrays are typically designed for a single direction (broadside) and ideal scanning by phase shifting is assumed. In practice, non-idealities such as beam deformation, beam squinting, mutual coupling and quantized phase shifters can cause severe beam degradation when scanning [33]. Additionally, the layout in aperiodic arrays is specifically designed to suppress radiation in unwanted directions, therefore scanning can pose additional difficulties. For these reasons it is desirable to include beam scanning effects in the design of phased arrays and cope with them in the best possible way.

Our initial approach (see Section 3.3) is based on the single beam optimization method which is now extended to the multi-beam case. By enforcing a new set of constraints for every additional beam we can guarantee compliance with the beam mask for each optimized beam, even in the presence of the above-described non-idealities. Since scanning degradation increases with angle, often few optimized beams suffice to guarantee a minimum deviation for all possible beams.

In this chapter classical phase scanning is introduced first and potential sources causing beam deformations are identified. Then, the proposed approach for simultaneous multi-beam optimization is discussed. The results of multi-beam optimization for a SATCOM scenario are discussed after-

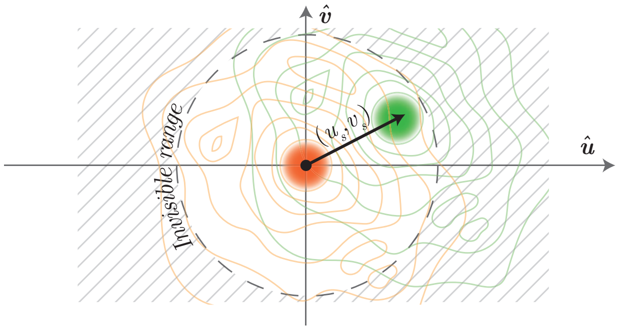

Figure 5.1: Phase scanning as $u - v$ space translation.

wards. Finally, a summary and the conclusions are given.

5.1 Classical Phase Scanning

Beam scanning can be obtained by phase tuning only. That is, given an arbitrary excitation set $\{w_n\}$, the associated pattern can be translated to the direction $\hat{\boldsymbol{r}}_s$ by modifying the excitation phases in accordance with

$$w_n^s = w_n e^{-jk\boldsymbol{r}_n \cdot \hat{\boldsymbol{r}}_s}. \tag{5.1}$$

Substituting the above expression in Eq. (2.3) gives

$$F^s(\hat{\boldsymbol{r}}) = \sum_{n=1}^{N} w_n^s e^{jk\boldsymbol{r}_n \cdot \hat{\boldsymbol{r}}} = \sum_{n=1}^{N} w_n e^{jk\boldsymbol{r}_n \cdot (\hat{\boldsymbol{r}} - \hat{\boldsymbol{r}}_s)} = \sum_{n=1}^{N} w_n e^{jk[x_n(u-u_s)+y_n(v-v_s)]} \tag{5.2}$$

where $u = \sin(\theta)\cos(\phi)$ and $v = \sin(\theta)\sin(\phi)$ are often referred to as sine or $u - v$ space. From the above expression it is clear that by linearly adjusting the element phases the pattern undergoes a translation in the $u - v$ space by the quantity (u_s, v_s), see also Fig. 5.1. This is valid for the Array Factor, while the element pattern is independent on the excitation.

Since the entire radiation pattern translates with the main beam, sidelobes, which before were outside the visible region, may enter the visible region when scanning. To design patterns that remain compliant with the SLL mask when scanning, enlarged sidelobe suppression regions commonly are used.

5.2 Beam Deformation

There are a number of causes for beam deformation when scanning. Some are intrinsic to antenna arrays, such as the mutual coupling effects, while others are due to the actual active components used to control the phases.

Translation

Phase scanning is a pure translation in the $u-v$ space, but the corresponding relationship in the $\theta - \phi$ space is non-linear. For this reason, the beam deforms when scanning. Beams are narrower in broadside and wider in the off-broadside direction due to the $\sin\theta$ relationship [33]. Additionally, a reduction in gain occurs as the equivalent aperture size decreases for larger scan angles. Hence, as the beam is scanned, the main beam widens and reduces in directivity while the side lobes get narrower and higher.

Mutual Coupling

As discusses in Chapter 4, mutual coupling can significantly modify the EEPs. In actual arrays, the different element patterns can result in a degradation of the scanned beam. Mutual coupling effects on the pattern are more pronounced for off-broadside directions since the radiation excites more strongly the neighbouring elements, therefore scanned beams are more sensitive to such effects.

Beam Squint

In Eq. (5.1) the phase varies linearly with frequency, thus the scanning direction is frequency invariant. A linear phase response is obtainable with time delays but more commonly phase shifters are used instead. In the latter case, the coefficient of Eq. (5.1) will be of the form,

$$w_n^s = w_n e^{-jk_d \boldsymbol{r}_n \cdot \hat{\boldsymbol{r}}_s}, \tag{5.3}$$

with $k_d = 2\pi/\lambda_d$ constant at the design frequency f_d. As a result, the beam deforms with frequency: above the design frequency, the scan angle becomes smaller then the intended one, and vice versa. This effect is referred to as *beam squint* [33].

Phase Quantization

Phase control is typically realized in a quantized way, resulting in some degradation due to the phase discretization error. Additionally, phase shifters can pose a significant cost driver, so that designers are interested in deploying cheaper low-resolution phase shifters. In such scenario the phase error due to quantization is not a small deviation but a considerable effect. Typically, phase errors manifest themselves as an increase in both the side and grating lobe levels [33].

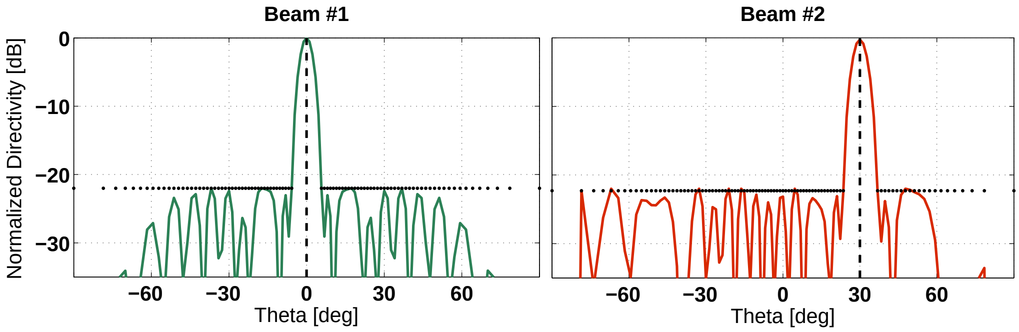

Figure 5.2: Illustration of multi-beam optimization: the array is simultaneously optimized for broadside (beam #1) and scanned (beam #2) directions.

5.3 Multi-Beam Optimization

The proposed method overcomes the limitations of conventional phase scanning approaches by optimizing the array for multi-beam applications. In phased arrays, the excitation coefficients and the expression for the pattern [Eq. (2.1)] can be defined in the general form

$$\boldsymbol{f}^p(\hat{\boldsymbol{r}}) = \sum_{n=1}^{N} w_n^p \boldsymbol{f}_n(\hat{\boldsymbol{r}}) \quad \text{with} \quad w_n^p = w_n e^{j\Phi_n^p}, \tag{5.4}$$

where Φ_n^p is the phase shift at element n for beam p.

For linear phase shift scanning in the direction of $\hat{\boldsymbol{r}}_p$, the corresponding phase shift term is $\Phi_n^p = -k\boldsymbol{r}_n \cdot \hat{\boldsymbol{r}}_p$. However, quantized phase shifters and non-linear frequency response can affect such values. To account for this, the phase shift can be modified to model such effects, e.g. by appropriate phase rounding for quantized phase shifters.

For P focused beam patterns scanning in the directions $\{\hat{\boldsymbol{r}}_p\}_{p=1}^{P}$ and prescribed radiation masks $\{M_\nu^p(\hat{\boldsymbol{r}})\}_{p=1}^{P}$ for the polarization component ν (see Fig. 5.2), the algorithm in (3.4) is modified to read [32]

$$\underset{\mathbf{w}^i \in \mathbb{C}^N}{\operatorname{argmin}} \|\mathbf{Z}^i \mathbf{w}^i\|_{\ell_1}, \text{ subject to } \begin{cases} f_{\mathrm{co}}^p(\hat{\boldsymbol{r}}_{\mathrm{p}}) = 1, & p = 1 \\ |f_\nu^p(\hat{\boldsymbol{r}})|^2 \leq M_\nu^p(\hat{\boldsymbol{r}}), & p = 1, ..., P \end{cases}. \tag{5.5}$$

The method optimizes the array layout and the complex excitations $\{w_n\}$ when an arbitrary number of scanned beams is considered simultaneously. This formulation allows to include any source causing beam degradation that can be modeled.

5.4 Results

The proposed multi-beam optimization approach will be demonstrated for a SATCOM scenario as introduced in Chapter 1. The results are summarized in Fig. 5.3. Three different array designs have been considered. For each one the array layout is shown together with the resulting far-field patterns when scanned to the far off-broadside direction in the D-plane $(8°, 45°)$. The far-field pattern cuts in the E, H and D-plane are shown together with its 2D contour representation.

The first array, shown in Fig. 5.3a, has been designed without accounting for the beam scanning. The array has been optimized for broadside scanning with a mask extending over the entire FoV ($\pm 8°$). The array is composed of 129 elements and has a broadside gain of 29.5 dBi. As expected, when the main beam is scanned far off-broadside, the side lobes violate the radiation mask with radiation levels as high as -12 dB.

The second array, shown in Fig. 5.3b, has been optimized for scanning using a conventional approach. To ensure full-range scanning, the array has been optimized at broadside with a mask extending twice that of the FoV (i.e. $\pm 16°$). For these specifications the number of elements is 305, with a resulting gain of 32.9 dBi. Despite the extended mask covers the whole FoV, also at far off-broadside directions, a SLL increase of about 5 dB is still observed.

The third and last array, shown in Fig. 5.3c, has been optimized for a multi-beam application using the proposed approach. Specifically, the array has been optimized for broadside and far scanned beams in the D plane, i.e., $\{(0°, 0°); (8°, 45°)\}$. For each optimized beam the mask extends only over the FoV since the effects of translation are included in the beam steering. The final array is composed of 385 elements and a gain of 34 dBi. The resulting far field patterns show that the algorithm successfully compensates for the beam degradation while the SLLs are guaranteed to be below the mask levels for any scanning direction.

5.5 Summary and Conclusions

In this chapter a method for the optimization of multi-beam antenna arrays has been presented. Conventional phased array designs assume undistorted pattern when scanning but, non-idealities, such as mutual coupling and phase shifter quantization error, can degrade the radiation pattern and cause higher SLL than desired. The proposed approach solves the problem by optimizing the array layout and excitations so as to provide well-behaved patterns for multiple beams simultaneously.

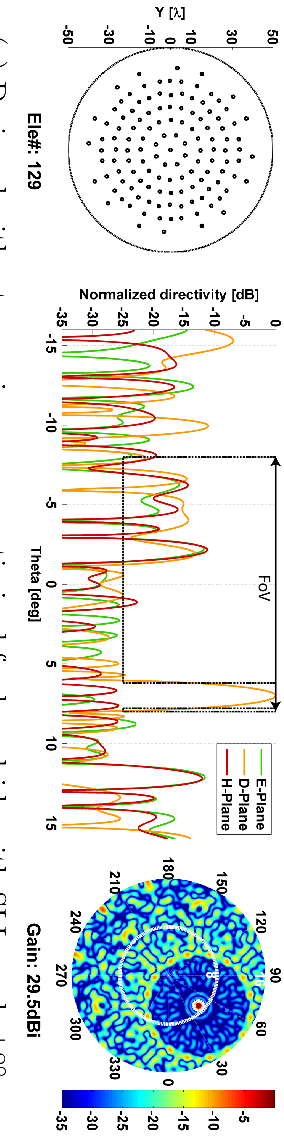

(a) Designed without scanning: array optimized for broadside with SLL mask ±8°

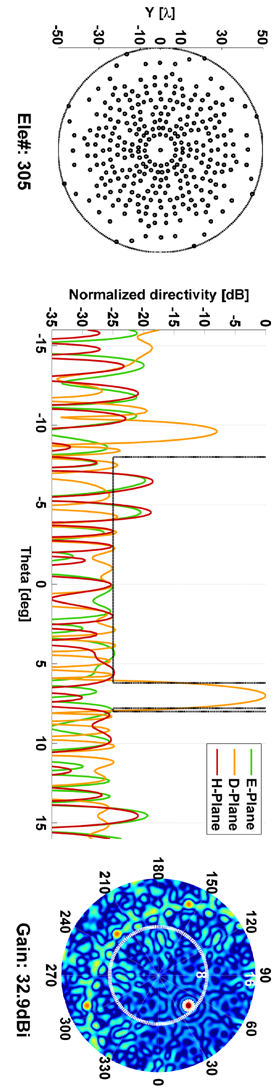

(b) Classical scanning design: array optimized for broadside with SLL mask ±16°

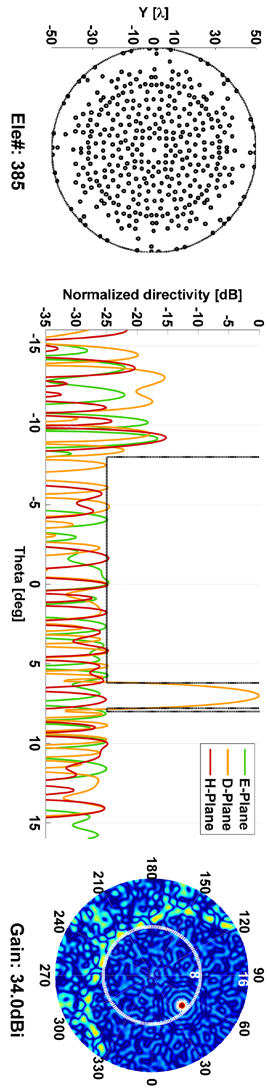

(c) Proposed scanning design: array optimized for broadside and far-off scanning $(\theta, \phi) = (8; 45)^\circ$ with SLL mask ±8°

Figure 5.3: Array layout and corresponding co-pol radiation pattern when scanning at $(\theta, \phi) = (8; 45)^\circ$

The results have been demonstrated for a SATCOM application by comparing a conventionally designed array to a multi-beam optimized phased array antenna. The approach is shown to compensate for beam degradation effects adequately and guarantees that the desired SLLs for each optimized beam are below the desired level. The improved scanning capabilities are obtained at the expense of an increase in the number of antenna elements.

The ability to include scanning degradation can be very important for the accurate design of multi-spot arrays. Additionally, the proposed multi-beam array synthesis approach allows designers to evaluate active components such as phase shifters and their effects on the final array design.

Chapter 6

Reducing Complexity Through Symmetry

Reducing the array complexity – and thus the associated cost – is paramount to next generation array antennas. This has been translated in the problem of designing MSAs as discussed in Chapter 3.

Minimizing the number of elements is of key importance, but may not always be the only aspect to consider. Layout and excitation symmetries, especially in large and complex arrays such as DRA:s, can be very beneficial in reducing the manufacturing costs [34]. In fact, component reuse and modular designs enable simpler and more economical solutions. Additionally, one can substantially simplify other aspects including the beamforming network and the thermal design [35]. For these reasons it is of great interest for designers to have the ability to impose and evaluate different types of layouts in order to find the most appropriate one for the specific application at hand.

Imposing a more regular design naturally reduces the aperiodicity of the array and reduces the solution space for the synthesis of the MSA. Accordingly, an increase in the number of elements can be expected. For practical applications the best compromise between modularity and the number of antennas is therefore preferred.

In this chapter we first describe the proposed approach to enforce and exploit the array and excitation symmetry. The formulation is general and applicable to a large class of symmetry types. Finally, the effects of rotational symmetry will be demonstrated when applied to a SATCOM application.

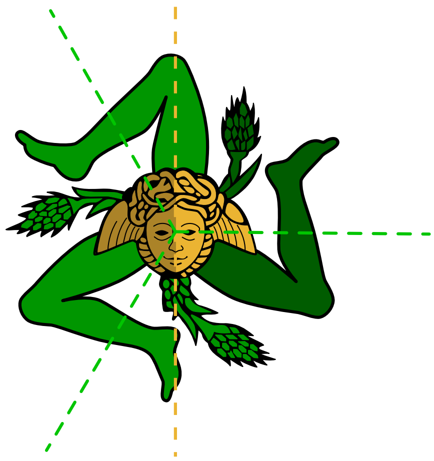

Figure 6.1: Trinacria, an example of a figure composed by two different symmetrical parts: a reflective (yellow) and a rotation (green) part.

6.1 Formulation

A geometry is said *symmetric* if it is invariant to some geometrical transformation, such as rotation, reflection or translation, as shown in Fig. 6.1 as an example.

Probably the most simple example of a symmetric layout is a linear array of identical elements. In such array, the elements are positioned symmetrically with respect to the center and excited in a conjugate symmetric way. For a classical array of an even number of elements, it is possible to simplify (2.3) as

$$\begin{aligned} F(\theta) &= w_1 e^{+jkx_1 \sin\theta} + w_1^* e^{-jkx_1 \sin\theta} + w_2 e^{+jkx_2 \sin\theta} + w_2^* e^{-jkx_2 \sin\theta} + ... \\ &= 2|w_1| \cos\left(kx_1 \sin\theta + \angle w_1\right) + 2|w_2| \cos\left(kx_2 \sin\theta + \angle w_2\right) + ... \end{aligned}$$

which relates the total array factor to the positive-x elements only.

The principle of combining the base (positive-x) element and the symmetrical (negative-x) element can be applied to an arbitrary array layout and set of element patterns. For the case of a vectorial far-field pattern, Eq. (2.1) can be expanded as,

$$\begin{aligned} \boldsymbol{f}(\hat{\boldsymbol{r}}) = & \ \{w_{1,1}\boldsymbol{f}_{1,1}(\hat{\boldsymbol{r}}) + w_{1,2}\boldsymbol{f}_{1,2}(\hat{\boldsymbol{r}}) + ...\} + \\ & \ \{w_{2,1}\boldsymbol{f}_{2,1}(\hat{\boldsymbol{r}}) + w_{2,2}\boldsymbol{f}_{2,2}(\hat{\boldsymbol{r}}) + ...\} + ... \\ = & \ w_1\{\tfrac{w_{1,1}}{w_1}\boldsymbol{f}_{1,1}(\hat{\boldsymbol{r}}) + \tfrac{w_{1,2}}{w_1}\boldsymbol{f}_{1,2}(\hat{\boldsymbol{r}}) + ...\} + \\ & \ w_2\{\tfrac{w_{2,1}}{w_2}\boldsymbol{f}_{2,1}(\hat{\boldsymbol{r}}) + \tfrac{w_{2,2}}{w_2}\boldsymbol{f}_{2,2}(\hat{\boldsymbol{r}}) + ...\} + ... \\ = & \ w_1\boldsymbol{f}_1(\hat{\boldsymbol{r}}) + w_2\boldsymbol{f}_2(\hat{\boldsymbol{r}}) + ... \end{aligned} \tag{6.1}$$

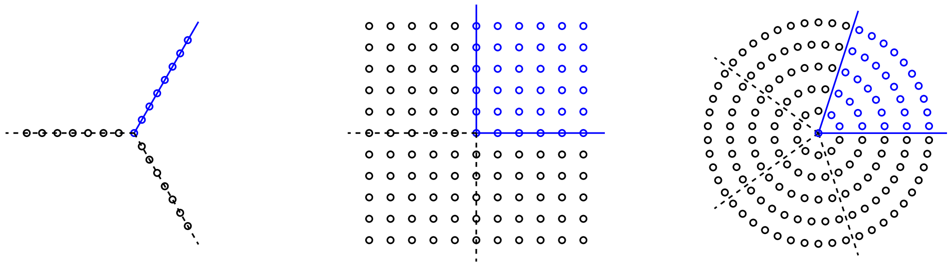

(a) Tri-linear (b) Rectangular quadrant (c) Circular sector

Figure 6.2: Examples of array layout symmetries, base elements in blue.

where $w_{n,s}$ and $\boldsymbol{f}_{n,s}$ are the excitation coefficient and far-field pattern of element n and symmetry region s, respectively, while w_n and $\boldsymbol{f}_n$ are the base excitation coefficient and equivalent far-field pattern obtained by summing the far-field pattern of the symmetric elements of n. That is, for the base element n with $N_{\text{sym}}(n)$ symmetrical elements and for a scanned beam p, the associated pattern can be written as

$$\boldsymbol{f}^p(\hat{\boldsymbol{r}}) = \sum_{n=1}^{N} w_n \boldsymbol{f}_n^p(\hat{\boldsymbol{r}}) \quad \text{with} \quad \boldsymbol{f}_n^p(\hat{\boldsymbol{r}}) = \sum_{s=1}^{N_{\text{sym}}(n)} \boldsymbol{f}_{n,s}(\hat{\boldsymbol{r}}) e^{-jk\Phi_{n,s}^p}. \tag{6.2}$$

Additionally, since the base element n represents now a collection of $N_{\text{sym}}(n)$ elements, its weight should be corrected for in the MSA optimization. Accordingly, in the iterative ℓ_1-norm minimization, Eq. (3.5) becomes:

$$z_m^i = \frac{1}{\sum_{s=1}^{N_{\text{sym}}(m)} |w_m^{(i-1)}| + \epsilon} = \frac{1}{N_{\text{sym}}(m)|w_m^{(i-1)}| + \epsilon}. \tag{6.3}$$

This general formulation can be applied to a very large number of symmetry types. Fig. 6.2 shows some examples including a linear, rectangular and circular sector. Additionally, composition of different symmetries (see Fig. 6.1) and pre-imposed amplitude taper can also be modeled, although this has not been investigated in this thesis.

6.2 Results

The effects of symmetries on the array design will be demonstrated for the SATCOM case-study that has been introduced in Chapter 1. Since for such a scenario the specifications are for a rotationally symmetric beam (ϕ-invariant), the natural choice of the layout is rotationally symmetric as well.

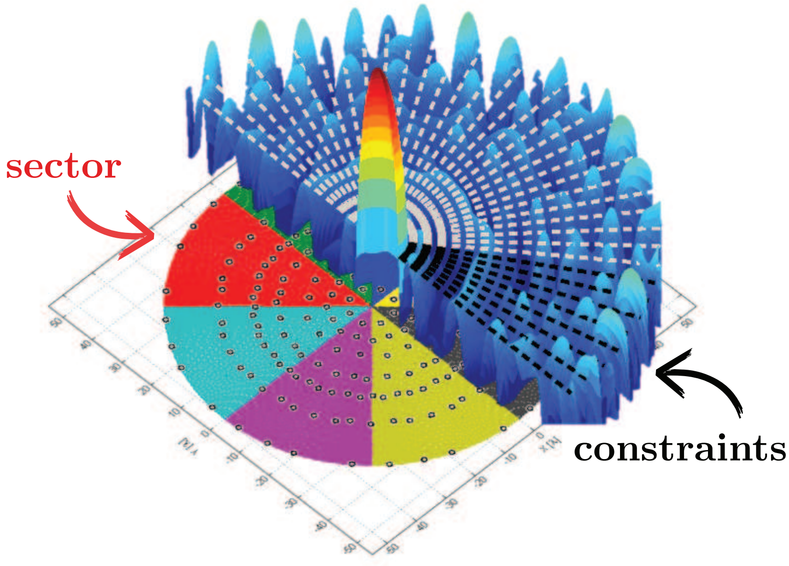

Figure 6.3: Array layout and far-field constraints for an 8-fold rotational symmetry. Only one sector of the aperture and of the pattern are considered.

For such type of symmetry the circular layout is divided in N_{sym} (i.e. order of symmetry) identical sectors, as shown in Fig. 6.3 for an 8-fold symmetry.

As discussed, only the base sector is considered during the sparsification phase, while the rest of the array is obtained by rotation. Additionally, since the symmetry is also found in the radiation pattern only one sector of the pattern needs to be considered. As a consequence, the synthesis problem size reduces like $1/N_{\mathrm{sym}}$ both in terms of the problem unknowns as well as the number of constraints, as shown in Fig. 6.3.

To study the effects of imposing symmetries, the array has been optimized for a 4-, 8-, 16- and 32-fold symmetry as well as without imposing any symmetry. Tab. 6.1 summarize the resulting layouts and far-field patterns, the number of elements, directivities and the total design times.

From the layout figures an increase in the regularity of the array and of the patterns is clearly visible. On the other hand, as the array modularity increases, so does the number of elements. The number of elements grows from 116 without symmetry to 193 for a 32-fold symmetry, an increase of about 2% per order of symmetry. The 8-fold case experiences a lower increase in the number of elements than expected (less than the 4-fold case). This is conjectured to be due to the approximated nature of the ℓ_1-norm minimization. Additionally, an increase in number of elements leads to an increased directivity, since the aperture filling and efficiency are higher for densely populated arrays. As discussed, the design time is also reduced proportional to $1/N_{\mathrm{sym}}^2$ due to the reduction both in the solution and constraint spaces.

6.3 Summary and Conclusions

In this chapter the problem of reducing the array complexity by means of enforcing and exploiting symmetries has been studied. Symmetrical arrays involve both the topology as well as the element excitations, therefore allowing modularity, component reuse and simplification of the layout and the beamforming network. The proposed formulation on imposing symmetries is kept general allowing for arbitrary types of symmetries by appropriate sampling of the array aperture.

The approach has been demonstrated in the synthesis of a rotationally symmetric circular array for a SATCOM application. Higher orders of symmetry allow for higher modularity, component reuse and simpler beamforming networks. However, an approximately linear increase in the number of elements with the the order of symmetry is to be expected.

The ability to impose arbitrary symmetries as is possible to greatly reduce the associated costs by conforming the array layout to the manufacturing process. Additionally, designers can investigate different symmetry orders and identify the one that is most cost-effective.

Symmetry order	none (reference)	4	8	16	32
Array layout	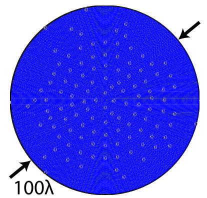	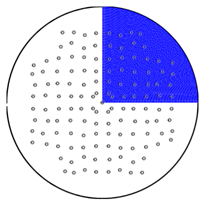	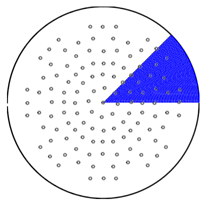	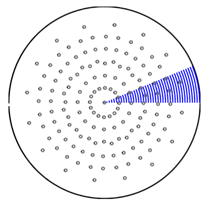	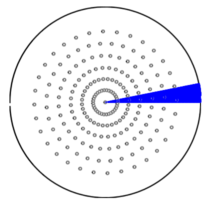
Broadside beam pattern	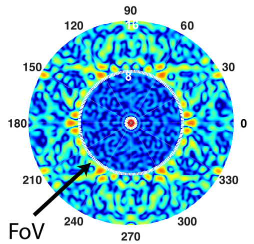	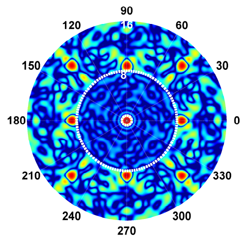	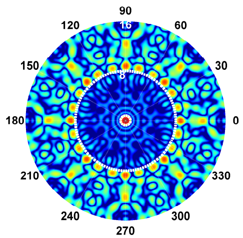	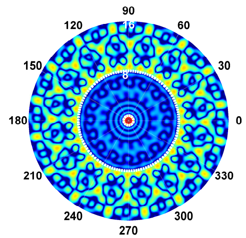	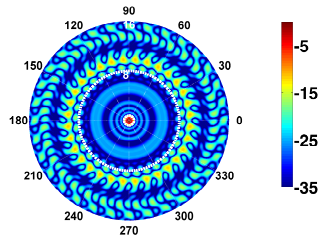
Element #	$N^{\{ref\}} = 116$	$N^{\{ref\}} + 17$ (15%)	$N^{\{ref\}} + 5$ (4%)	$N^{\{ref\}} + 29$ (25%)	$N^{\{ref\}} + 80$ (69%)
Directivity	$D^{\{ref\}} = 29.19$dBi	$D^{\{ref\}} + 0.3$dB	$D^{\{ref\}} + 0.1$dB	$D^{\{ref\}} + 0.4$dB	$D^{\{ref\}} + 0.9$dB
Design time	$t^{\{ref\}} = 48$h36m	$t^{\{ref\}}/16$	$t^{\{ref\}}/64$	$t^{\{ref\}}/256$	$t^{\{ref\}}/4096$

Table 6.1: Array layout for increasing rotational symmetry orders

Chapter 7

Contributions and Future Work

Aperiodic array synthesis is a highly active research topic: designing advanced arrays with the minimum number of antenna elements is attractive but also challenging. Several synthesis methods have been proposed, yet aperiodic array design techniques are not as mature as those in use for their regular array counterparts. They are either: (i) accurate but computationally-expensive (e.g. Genetic Optimization techniques), or; (ii) efficient but simplified (e.g. analytical techniques).

In this thesis we have presented a new method based on the theory of Compressive Sensing for the efficient design of arrays of complex antenna elements that meet stringent performance specifications. The major contributions of this work include:

- The recently published iterative ℓ_1-optimization method has been extended to the design of irregular arrays in the presence of Mutual Coupling effects. Antenna coupling effects are sometimes neglected in order to simplify the synthesis procedure, although they can have significant effects. To include MC effects, the proposed method has been hybridized with a rigorous full-wave analysis which iteratively refines the array layout and excitation scheme in few iterations, therefore making it an effective solution, also for large arrays. Results have been shown for a small linear array of strongly coupled dipole elements as well as a large planar array of horn antenna elements.
- Multi-beam optimization has been included in the array synthesis framework. In conventional approaches, phased arrays are designed for one direction only, while ideal scanning behavior is assumed. In practice, beam deformation can arise due to antenna MC effects and quantized phase shifters, causing the beam to potentially violate the SLL requirement when scanning. The proposed method addresses the problem for multi-spot applications by simultaneously optimizing for

multiple scanning directions and SLL masks. Results show that the method successfully corrects the scanning degradations, guaranteeing that the SLL constraints are met for every optimized beam.

- The effects of layout and excitation symmetries have been studied. Enforcing and subsequently exploiting array symmetries can be very beneficial in terms of design modularity, component reuse and simplification of both the array design and excitation scheme, with an important reduction in the overall costs. The method has been formulated for a generic symmetry type and demonstrated in the synthesis of rotationally symmetric circular arrays. Results demonstrate that the number of antenna elements increases with higher degree of modularity.

7.1 Future Work

The array synthesis framework presented in this thesis is generic and flexible and therefore well-suited to be used also for other applications and can be easily extended. Some additional aspects worth investigating and including in the optimization of the array systems are given below.

Multi-type element arrays have the potential to further improve the design. Other authors have investigated this approach with deterministic approaches and found that by using a set of elements of different sizes it is possible to further reduce the number of elements while increasing the aperture efficiency, albeit at the expense of the ability to scan. From an optimization point of view, the use of multiple element types represents an additional degree of freedom which can be exploited. It is of interest studying how this approach could be included in the proposed optimization method.

Amplitude level control is an important aspect to consider when designing energy efficient active arrays. Solid state amplifiers have best efficiency when working in saturation and should therefore be used in such condition. Several design techniques consider only single level excitations (isophoric), although a small number of amplifier types could be employed for increased flexibility. At present, the proposed method does not offer the ability to directly choose the number of amplitude control levels, only indirectly by enforcing symmetries. For this reason it would be of interest to extend the method to arbitrary but discrete amplitude level controls.

References

[1] A. Ellgadt, L. Jonsson, M. Ivashina, R. Maaskant, M. Lanne, J. Carlert, P. Ingvarsson, B. Johassisson, P. Persson, L. Pettersson, and T. Boman, "Next generation arrays antennas," Chase Stage III Project Proposal, Sep. 2011.

[2] ESA/ESTEC, "Innovative architectures for reducing the number of controls of multiple beam telecommunications antennas," Tender AO/1-5598/08/NL/ST, Jan. 2008.

[3] P. Ingvarson and J. Zackrisson, "Swedish space antenna projects," in *Antennas and Propagation (EuCAP), 2013 7th European Conference on*, April 2013, pp. 3161–3165.

[4] H. Unz, "Linear arrays with arbitrarily distributed elements," *Antennas and Propagation, IRE Transactions on*, vol. 8, no. 2, pp. 222–223, 1960.

[5] R. L. Haupt, "Thinned arrays using genetic algorithms," *IEEE Trans. Antennas Propag.*, vol. 42, no. 7, pp. 993–999, 1994.

[6] M. M. Khodier and C. G. Christodoulou, "Linear array geometry synthesis with minimum sidelobe level and null control using particle swarm optimization," *IEEE Trans. Antennas Propag.*, vol. 53, no. 8, pp. 2674–2679, 2005.

[7] Óscar Quevedo-Teruel and E. Rajo-Iglesias, "Ant colony optimization in thinned array synthesis with minimum sidelobe level," *IEEE Antennas Wireless Propag. Lett.*, vol. 5, no. 1, pp. 349–352, 2006.

[8] G. G. Roy, S. Das, P. Chakraborty, and P. N. Suganthan, "Design of non-uniform circular antenna arrays using a modified invasive weed optimization algorithm," *IEEE Trans. Antennas Propag.*, vol. 59, no. 1, pp. 110–118, 2011.

[9] G. Oliveri, F. Caramanica, and A. Massa, "Hybrid ads-based techniques for radio astronomy array design," *IEEE Trans. Antennas Propag.*, vol. 59, no. 6, pp. 1817–1827, 2009.

[10] M. Andreasen, “Linear arrays with variable interelement spacings,” *Antennas and Propagation, IRE Transactions on*, vol. 10, no. 2, pp. 137–143, 1962.

[11] A. Ishimaru, “Theory of unequally-spaced arrays,” *Antennas and Propagation, IRE Transactions on*, vol. 10, no. 6, pp. 691–702, 1962.

[12] Y. Lo, “A mathematical theory of antenna arrays with randomly spaced elements,” *IEEE Trans. Antennas Propag.*, vol. 12, no. 3, pp. 257–268, 1964.

[13] Y. Lo and S.-W. Lee, “A study of space-tapered arrays,” *IEEE Trans. Antennas Propag.*, vol. 14, no. 1, pp. 22–30, 1966.

[14] B. Steinberg, “Comparison between the peak sidelobe of the random array and algorithmically designed aperiodic arrays,” *IEEE Trans. Antennas Propag.*, vol. 21, no. 3, pp. 366–370, 1973.

[15] Y. Liu, Z. Nie, and Q.-H. Liu, “Reducing the number of elements in a linear antenna array by the matrix pencil method,” *Antennas and Propagation, IEEE Transactions on*, vol. 56, no. 9, pp. 2955–2962, 2008.

[16] G. Oliveri, M. Donelli, and A. Massa, “Linear array thinning exploiting almost difference sets,” *IEEE Trans. Antennas Propag.*, vol. 57, no. 12, pp. 3800–3812, 2009.

[17] D. Caratelli and M. Vigano, “A novel deterministic synthesis technique for constrained sparse array design problems,” *IEEE Trans. Antennas Propag.*, vol. 59, no. 11, pp. 4085–4093, Nov 2011.

[18] A. Ishimaru, “Unequally spaced arrays based on the poisson sum formula,” *IEEE Trans. Antennas Propag.*, vol. 62, no. 4, pp. 1549–1554, April 2014.

[19] W. P. M. N. Keizer, “Large planar array thinning using iterative fft techniques,” *IEEE Trans. Antennas Propag.*, vol. 57, no. 10, pp. 3359–3362, Oct 2009.

[20] O. Bucci, S. Perna, and D. Pinchera, “Advances in the deterministic synthesis of uniform amplitude pencil beam concentric ring arrays,” *IEEE Trans. Antennas Propag.*, vol. 60, no. 7, pp. 3504–3509, 2012.

[21] M. A. Davenport, M. F. Duarte, Y. C. Eldar, and G. Kutyniok, “Introduction to compressed sensing,” *Preprint*, vol. 93, 2011.

[22] A. Massa, P. Rocca, and G. Oliveri, "Compressive sensing in electromagnetics-a review," *IEEE Antennas Propag. Mag.*, vol. 57, no. 1, pp. 224–238, 2015.

[23] G. Prisco and M. D'Urso, "Maximally sparse arrays via sequential convex optimizations," *IEEE Antennas Wireless Propag. Lett.*, vol. 11, pp. 192–195, 2012.

[24] P. Kildal, *Foundations of Antennas: A Unified Approach*, 2015. [Online]. Available: http://www.kildal.se/

[25] C. Bencivenni, M. Ivashina, and R. Maaskant, "A simple method for optimal antenna array thinning using a broadside maxgain beamformer," in *Antennas and Propagation (EuCAP), 2013 7th European Conference on*, April 2013, pp. 1799–1802.

[26] S. E. Nai, W. Ser, Z.-L. Yu, and H. Chen, "Beampattern synthesis for linear and planar arrays with antenna selection by convex optimization," *IEEE Trans. Antennas Propag.*, vol. 58, no. 12, pp. 3923–3930, 2010.

[27] L. Cen, Z. L. Yu, and W. Ser, "Antenna array synthesis in presence of mutual coupling effect for low cost implementation," in *Integrated Circuits, ISIC '09. Proceedings of the 2009 12th International Symposium on*, Dec 2009, pp. 360–363.

[28] D. Pozar, "The active element pattern," *IEEE Trans. Antennas Propag.*, vol. 42, no. 8, pp. 1176–1178, Aug 1994.

[29] R. Maaskant, C. Bencivenni, and M. Ivashina, "Characteristic basis function analysis of large aperture-fed antenna arrays," in *Antennas and Propagation (EuCAP), 2014 8th European Conference on*, April 2014, pp. 2427–2431.

[30] C. Bencivenni, M. Ivashina, S. Maaskant, and J. Wettergren, "Design of maximally sparse antenna arrays in the presence of mutual coupling," *IEEE Antennas Wireless Propag. Lett.*, vol. 159-162, pp. 1–1, 2015.

[31] R. Maaskant, "Analysis of large antenna systems," Ph.D. dissertation, Eindhoven University of Technology, Eindhoven, 2010. [Online]. Available: http://alexandria.tue.nl/extra2/201010409.pdf

[32] C. Bencivenni, M. Ivashina, S. Maaskant, and J. Wettergren, "Fast synthesis of wide-scan-angle maximally sparse array antennas using compressive-sensing and full-wave em-analysis," *IEEE Trans. Antennas Propag.*, submitted April 2015.

[33] R. J. Mailloux, *Phased array antenna handbook.*

[34] RUAG Space A.B., Personal discussion, 2014.

[35] A. Catalani, L. Russo, T. Isernia, O. M. Bucci, G. Toso, and P. Angeletti, "Ka-band active sparse arrays for satcom applications," in *Antennas and Propagation Society International Symposium (APSURSI), 2012 IEEE*, Jun. 2012, pp. 1–2.